National Library of Canada
Acquisitions and Bibliographic Services Branch
395 Wellington Street
Ottawa, Ontario
K1A 0N4

Bibliothèque nationale du Canada
Direction des acquisitions et des services bibliographiques
395, rue Wellington
Ottawa (Ontario)
K1A 0N4

Your file Votre référence

Our file Notre référence

NOTICE

The quality of this microform is heavily dependent upon the quality of the original thesis submitted for microfilming. Every effort has been made to ensure the highest quality of reproduction possible.

If pages are missing, contact the university which granted the degree.

Some pages may have indistinct print especially if the original pages were typed with a poor typewriter ribbon or if the university sent us an inferior photocopy.

Reproduction in full or in part of this microform is governed by the Canadian Copyright Act, R.S.C. 1970, c. C-30, and subsequent amendments.

AVIS

La qualité de cette microforme dépend grandement de la qualité de la thèse soumise au microfilmage. Nous avons tout fait pour assurer une qualité supérieure de reproduction.

S'il manque des pages, veuillez communiquer avec l'université qui a conféré le grade.

La qualité d'impression de certaines pages peut laisser à désirer, surtout si les pages originales ont été dactylographiées à l'aide d'un ruban usé ou si l'université nous a fait parvenir une photocopie de qualité inférieure.

La reproduction, même partielle, de cette microforme est soumise à la Loi canadienne sur le droit d'auteur, SRC 1970, c. C-30, et ses amendements subséquents.

Canada

University of Alberta

A NEW MATHEMATICAL MODEL FOR ONE-DIMENSIONAL MISCIBLE DISPLACEMENT

by

Jiasen Tan

A thesis submitted to the Faculty of Graduate Studies and Research in partial fulfillment of the requirements for the degree of Master of Science

in

Petroleum Engineering

Department of Mineral, Metallurgical and Petroleum Engineering

Edmonton, Alberta

Fall 1995

National Library
of Canada

Acquisitions and
Bibliographic Services Branch

395 Wellington Street
Ottawa, Ontario
K1A 0N4

Bibliothèque nationale
du Canada

Direction des acquisitions et
des services bibliographiques

395, rue Wellington
Ottawa (Ontario)
K1A 0N4

Your file Votre référence

Our file Notre référence

THE AUTHOR HAS GRANTED AN IRREVOCABLE NON-EXCLUSIVE LICENCE ALLOWING THE NATIONAL LIBRARY OF CANADA TO REPRODUCE, LOAN, DISTRIBUTE OR SELL COPIES OF HIS/HER THESIS BY ANY MEANS AND IN ANY FORM OR FORMAT, MAKING THIS THESIS AVAILABLE TO INTERESTED PERSONS.

L'AUTEUR A ACCORDE UNE LICENCE IRREVOCABLE ET NON EXCLUSIVE PERMETTANT A LA BIBLIOTHEQUE NATIONALE DU CANADA DE REPRODUIRE, PRETER, DISTRIBUER OU VENDRE DES COPIES DE SA THESE DE QUELQUE MANIERE ET SOUS QUELQUE FORME QUE CE SOIT POUR METTRE DES EXEMPLAIRES DE CETTE THESE A LA DISPOSITION DES PERSONNE INTERESSEES.

THE AUTHOR RETAINS OWNERSHIP OF THE COPYRIGHT IN HIS/HER THESIS. NEITHER THE THESIS NOR SUBSTANTIAL EXTRACTS FROM IT MAY BE PRINTED OR OTHERWISE REPRODUCED WITHOUT HIS/HER PERMISSION.

L'AUTEUR CONSERVE LA PROPRIETE DU DROIT D'AUTEUR QUI PROTEGE SA THESE. NI LA THESE NI DES EXTRAITS SUBSTANTIELS DE CELLE-CI NE DOIVENT ETRE IMPRIMES OU AUTREMENT REPRODUITS SANS SON AUTORISATION.

ISBN 0-612-06544-8

Canada

University of Alberta

Library Release Form

Name of Author: Jiasen Tan

Title of Thesis: *A NEW MATHEMATICAL MODEL FOR ONE-DIMENSIONAL MISCIBLE DISPLACEMENT*

Degree: Master of Science

Year this Degree Granted: 1995

Permission is hereby granted to the University of Alberta Library to reproduce single copies of this thesis and to lend or sell such copies for private, scholarly, or scientific research purposes only.

The author reserves all other publication and other rights in association with the copyright in the thesis, and except as hereinbefore provided, neither the thesis nor any substantial portion thereof may be printed or otherwise reproduced in any material form whatever without the author's prior written permission.

Jiasen Tan
.....

606 Chemical Building
University of Alberta
Edmonton, Alberta
Canada T6G 2G6

DATED Oct. 5, 1995 .....

University of Alberta

Faculty of Graduate Studies and Research

The undersigned certify that they have read, and recommend to the Faculty of Graduate Studies and Research for acceptance, a thesis entitled *A NEW MATHEMATICAL MODEL FOR ONE-DIMENSIONAL MISCIBLE DISPLACEMENT* submitted by Jiasen Tan in partial fulfillment of the requirements for the degree of Master of Science in Petroleum Engineering.

Dr. R. Bentsen (Supervisor)

Dr. K. Barron (Chairman, examiner)

Dr. A. Ambastha (Examiner)

Dr. R. E. Hayes (External examiner)

Date approved: Sept. 15/95

ABSTRACT

Based on Darcy's law, Fick's dispersion law and the continuity equation, a new mathematical model for one-dimensional miscible displacement has been developed. To analyze the effects of the parameters included in the model, an approximate analytical solution to the model was found. Furthermore, a theoretical analysis based on linear perturbation theory, together with the new model, has been made to derive a dimensionless scaling group to predict the onset of instability. The experimentally determined effluent curves of miscible displacements were compared with the theoretical results which were calculated using the new model.

It was found from the approximate analytical solution that the transition zone grows with the square root of time at early stages when dispersion dominates. As a displacement goes on, the transition zone grows linearly with time when the effect of dispersion is negligible. Experimental data published in the literature confirmed this phenomenon [Withjack, 1988]. Through effluent history match calculations, it is shown that the effective viscosity ratio and the dispersion coefficient increase with increasing flow rate, and the dispersion coefficient decreases as the viscosity difference becomes larger.

ACKNOWLEDGEMENTS

The author would like to express his sincere gratitude to Dr. Ramon G. Bentsen, Professor of Petroleum Engineering, for his guidance and supervision. Without his support, this investigation could not have been completed.

Acknowledgements are also made to the Natural Sciences and Engineering Research Council of Canada (NSERC) for financial support.

Special thanks should be given to Mr. Ning Liu, director of the PVT and Miscible Flooding Laboratory, RIPED, China, under whose permission, some experimental equipment and chemicals were provided to conduct the experiments.

CONTENTS

Chapter		Page
1.	Introduction	1
2.	Literature Review	4
3.	Statement of the Problem	11
4.	Theory	13
4.1	Generalized Dispersion-Convection Equation	13
4.2	Effective Viscosity Ratio	19
4.3	Heterogeneity Factor	19
4.4	The Function F_S	20
4.5	Dimensionless Form	21
4.6	Initial and Boundary Conditions	22
4.7	Comparison with Existing Theories	23
4.8	Numerical Solution to the Proposed Model	24
4.8.1	Concentration of Displacing Fluid in Effluent	25
4.8.2	Transition Zone Length	26
5.	Approximate Analytical Solution	31
5.1	Transition Zone Growth	31
5.2	Procedure for Calculating f_S	39
5.3	Comparison with Numerical Solution	40
6.	Comparison with Published Data	47
6.1	Comparison with Brigham et al.'s Data	47
6.2	Comparison with Withjack's Data	48
7.	Prediction of the Onset of Instability	53

7.1 Basic Equations 53
7.2 Small Perturbation Theory 55
7.3 Marginal Instability 57
7.4 Comparison with Coskuner and Bentsen's Theory 64
8. Experimental 67
8.1 Description of Experimental Apparatus 67
8.2 Experimental Procedures 68
9. Experimental Results and Discussion 73
9.1 Comparison of Effluent Curves with Theoretical Predictions 73
9.1.1 Displacements with Favorable Viscosity Ratios 74
9.1.2 Displacements with Unfavorable Viscosity Ratios 77
9.2 Breakthrough Recovery 78
9.3 Effective Viscosity Ratio 81
9.4 Dispersion Coefficient 82
9.5 Effect of Flow Velocity and Viscosity Ratio on Effluent Curve 84
9.6 Discussion of Errors 86
10. Summary and Conclusions 99
11. Suggestions for Future Study 101
12. References 102
13. Appendix A 105

LIST OF TABLES

Table		Page
9.1	Properties of the Miscible Fluids	88
9.2	Breakthrough Recovery: Experimental and Matched	89

LIST OF FIGURES

Figure ..... Page

4.1 One Dimensional Porous Medium 28

4.2 Sample Calculations of Effluent Histories Using Numerical Method 29

4.3 Transition Zone Length Growth from Numerical Solutions 30

5.1 Integration of Equation (5.17) versus HE 42

5.2 Half Transition Zone Length Growth Using Approximate Analytical Scheme 43

5.3 Effluent History Using Numerical and Approximate Schemes (HE=1) 44

5.4 Effluent History Using Numerical and Approximate Schemes (HE=1.25) 45

5.5 Effluent History Using Numerical and Approximate Schemes (HE=2) 46

6.1 Comparison of Effluent Curve of Brigham's Data with

Numerical Solution 50

6.2 Comparison of Effluent Curves of Withjack's Data with Approximate Analytical Solution 51

6.3 Comparison of Normalized Distance of Withjack's Data with Approximate Analytical Solution 52

7.1 A Downward Miscible Displacement 66

8.1 Schematic Drawing of Experimental Apparatus 70

8.2 Viscosity of Glycerine Solution 71

8.3 Refractive Index of Glycerine Solution 72

9.1 Effluent Curves of Displacements Using Fluids with Favorable Viscosity Ratios 90

9.2 Transition Zone Growth with Time Using Different Models 91

9.3 Effluent Curves: Experimental versus Predicted Viscosity ratio=4.15 92

9.4 Effluent Curves: Experimental versus Predicted Viscosity ratio=36.59 93

9.5 Effective Viscosity Ratio Changes with Velocity 94

9.6 Dispersion Coefficient Changes with Viscosity Ratio 95

9.7 Dispersion Coefficient Changes with Velocity 96

9.8 Effluent Curves for Different Displacement Velocities 97

9.9 Effluent Curves for Different Viscosity Ratios 98

A.1 Effluent Curves: Experimental versus Matched

Viscosity Ratio=4.15, Velocity=0.00188 cm/s 106

A.2 Effluent Curves: Experimental versus Matched

Viscosity Ratio=4.15, Velocity=0.00300 cm/s 107

A.3 Effluent Curves: Experimental versus Matched

Viscosity Ratio=8.54, Velocity=0.00038 cm/s 108

A.4 Effluent Curves: Experimental versus Matched

Viscosity Ratio=8.54, Velocity=0.00075 cm/s 109

A.5 Effluent Curves: Experimental versus Matched

Viscosity Ratio=8.54, Velocity=0.00113 cm/s 110

A.6 Effluent Curves: Experimental versus Matched

Viscosity Ratio=36.59, Velocity=0.00038 cm/s 111

NOMENCLATURE

a	A parameter defined by Equation (5.27)
A	Cross-sectional area, m^2
A_m	Variational coefficients
b	A parameter defined by Equation (5.28)
c	Solvent concentration, dimensionless
$\bar{c}$	Unperturbed solvent concentration, dimensionless
c^*	Solvent concentration perturbation, dimensionless
$\tilde{c}(z)$	Amplitude of solvent concentration perturbation, dimensionless
D_L	Longitudinal dispersion coefficient, m^2/s
D_T	Transverse dispersion coefficient, m^2/s
E	Effective viscosity ratio, dimensionless
f_o	Fractional flow of oil in effluent, dimensionless
f_s	Fractional flow of solvent in effluent, dimensionless
F_s	Fractional flow of solvent in effluent caused by convection, dimensionless
g	Gravitational acceleration, m/s^2
H	Heterogeneity factor of the porous medium, dimensionless

I	Instability number, dimensionless
k	Absolute permeability, m^2
K	Ratio of transverse to longitudinal dispersion coefficients, dimensionless
L	Length of the porous medium, m
L_x	Width of the porous medium, m
L_y	Height of the porous medium, m
M	Gradient of the natural logarithm of unperturbed viscosity, m^{-1}
p	Pressure, Pa
$\bar{p}$	Unperturbed pressure, Pa
p^*	Pressure perturbation, Pa
$\tilde{p}(z)$	Amplitude of pressure perturbation, Pa
P_e	Peclet number, dimensionless
q	Total volumetric flow rate, m^3/s
q_o	Volumetric flow rate of oil, m^3/s
q_s	Volumetric flow rate of solvent, m^3/s
q_{oD}	Volumetric flow rate of oil caused by dispersion, m^3/s
q_{ov}	Volumetric flow rate of oil caused by convection, m^3/s

q_{sD} Volumetric flow rate of solvent caused by dispersion, m^3/s

q_{sv} Volumetric flow rate of solvent caused by convection, m^3/s

R_b Experimentally measured breakthrough recovery, dimensionless

R_{bc} Calculated breakthrough recovery, dimensionless

t Real time, s

u Velocity in the x-direction, m/s

$\bar{u}$ Unperturbed velocity in the x-direction, m/s

u^* Perturbation velocity in the x-direction, m/s

v Velocity in the y-direction, m/s

$\bar{v}$ Unperturbed velocity in the y-direction, m/s

v^* Perturbation velocity in the y-direction, m/s

V Displacement velocity, m/s

V_k Permeability variation coefficient defined by Walsh et al. [1993], dimensionless

w Velocity in the z-direction, m/s

$\bar{w}$ Unperturbed velocity in the z-direction, m/s

w^* Perturbation velocity in the z-direction, m/s

$\tilde{w}(z)$	Amplitude of velocity perturbation in the z-direction, m/s
z	Moving coordinate
z'	Stationary coordinate
γ	Wave number, m^{-1}
δ_{mn}	Dirac delta function
ξ	Any perturbed dependent variable
$\bar{\xi}$	Any unperturbed dependent variable
ξ^*	Perturbation to any of the dependent variables
$\tilde{\xi}(z)$	Amplitude of perturbation to any of the dependent variables
μ	Viscosity, Pa.s
$\bar{\mu}$	Unperturbed viscosity, Pa.s
μ^*	Perturbation viscosity, Pa.s
μ_o	Oil viscosity, Pa.s
μ_s	Solvent viscosity, Pa.s
ρ	Density, kg/m^3
$\bar{\rho}$	Unperturbed density, kg/m^3
ρ^*	Perturbation density, kg/m^3

ρ_o	Oil density, kg/m^3
ρ_s	Solvent density, kg/m^3
τ	Pore volumes injected, dimensionless
τ_b	Breakthrough recovery, dimensionless
Ψ	Function defined by Equation (7.6), dimensionless
ϕ	Porosity, dimensionless
Ω	Dimensionless length

1. INTRODUCTION

As the cost of petroleum exploration increases, it becomes desirable to recover more oil from already-found oil reservoirs. Because ordinary water flooding leaves approximately 50 to 60 per cent of the original oil unrecovered, various enhanced oil recovery methods have become more and more important. Miscible displacement attracts people's attention because very high recovery can be obtained from the contacted parts of a reservoir. But the development of miscible flooding projects is slow due to the very large investment required and the uncertainty of oil production performance.

The uncertainty associated with the oil production performance arises out of fingering and gravity tonguing of the less viscous and less heavy miscible solvent into the reservoir fluid, which causes severe reduction of the volumetric sweep efficiency [Stalkup, 1984]. This phenomenon becomes more complicated when the heterogeneity of the reservoir is taken into account [Hewett and Behrens, 1993].

To decrease the expenditure involved, a principal solvent slug, which is miscible with the in-situ reservoir oil, is chased by a cheap solvent which is miscible with the principal solvent, but not with the oil. Because of dispersion between the principal solvent and the oil, as well as between the solvent and the chasing solvent, the principal solvent slug is diluted to a level below which it can be miscible with the reservoir fluid. So, it is very important to predict the extent of dispersion or mixing as the solvent slug travels through the reservoir formation.

The difference in miscible solvent components and operating conditions divides the process into two categories. When the injection fluids for miscible displacement mix directly with reservoir oils in all proportions and their mixtures remain single phase, they are called "first-contact-miscible". Some other injection

fluids, although they are not first-contact-miscible with reservoir fluids, can also form a continuous transition zone of fluid compositions that ranges from oil to injection fluid composition, through a series of in-situ mass transfers of the components between the reservoir oil and the injection fluid. Miscibility achieved by in-situ mass transfer of components resulting from repeated contact of oil and injection fluid during flow is called "multiple contact" or dynamic miscibility [Stalkup, 1984].

As compared to immiscible displacement, first contact miscible flooding has a very distinct characteristic: there is no interface between the displacing and the displaced fluid. Consequently, it is not necessary to consider the effect of capillary forces as one has to for immiscible flooding. But another phenomenon, dispersion or mixing between the injection solvent and the reservoir oil, which affects the displacement performance, must be taken into account in addition to the pressure force.

Great efforts have been made to develop mathematical models to describe miscible displacement adequately [Dougherty, 1963; Koval, 1963; Perrine, 1963; Deans, 1963; Coats and Smith, 1964; Nguyen and Bagster, 1979; Fayers, 1984; Vossoughi et al., 1984; Udey and Spanos, 1991; Udey and Spanos, 1993; Walsh and Withjack, 1993] . There are basically three types of mathematical models for miscible displacement. The first one is the standard theory which is a combination of Fick's law and the continuity equation. Based on this theory, the transition zone length grows with the square root of time. Some recent experiments have demonstrated that this is not always true [Walsh and Withjack, 1993]. Furthermore, the value of the dispersion coefficient needed by a simulation to match an actual field scale miscible displacement is usually much larger than that obtained from the breakthrough curves of core flooding in the laboratory [Pickens and Grisak, 1981].

Therefore, the dispersion is apparently scale dependent. The second approach is to use immiscible two-phase flow theory for miscible displacement, which means that dispersion is totally neglected. Based on this theory, the transition zone length grows linearly with time. Obviously, this theory approaches the correct solution only when the flow rate is great enough or other variables such as heterogeneity of the porous medium and the properties of the fluids make convection dominate the process. In fact, dispersion plays a very important role during miscible displacement [Blackwell et al., 1959]. Finally, the third approach is to combine the effects of dispersion and convection.

The purpose of this study is to use the third approach to derive a mathematical model for miscible displacement, which includes the viscosity ratio of the fluids and the heterogeneity of the porous medium explicitly in the model. Then, the model is used to match the experimental data taken in this study and published in the literature. Moreover, by incorporating linear perturbation theory with the new model, an attempt is made to derive a dimensionless scaling group for the theoretical prediction of the onset of instability of a miscible displacement conducted in a heterogeneous porous medium.

2. LITERATURE REVIEW

First contact miscible displacement, theoretically speaking, can recover 100% of the contacted oil due to the fact that there is no interface between the displaced oil and the injected solvent. But, in practice, the viscosity difference of the oil and solvent and the heterogeneity of the porous medium decrease the sweep efficiency to such an extent that miscible displacement is no longer attractive or profitable. In addition to the traditional convection-dispersion equation, which was derived from Fick's first diffusion law and valid only for matched miscible fluids and homogeneous porous media [Aris and Amundson, 1957], some different mathematical models have been proposed, which are capable of taking into account unmatched densities and viscosities and the non-uniform properties of the porous medium. Because of the very large number of papers in the literature, only major works are reviewed in this section.

When the Fickian dispersion law is employed to describe the mixing effects of matched fluids in a uniform porous medium, one obtains the traditional convection-dispersion equation [Aris and Amundson, 1957], which is given as Equation (2.1):

$$- (v \,.\, \nabla c) + \nabla \,.\, (D \,.\, \nabla c) = \frac{\partial c}{\partial t} \,. \qquad (2.1)$$

In a semi-infinite, one dimensional system, the above equation has an error function type solution [Brigham, 1974]. When the Dirichlet condition at the inlet and the Neumann condition at the outlet end are applied for a finite system, the solution has the form of an infinite series of error functions, where the successive terms arise

from superimposed reflections at the outlet end [Oguztoreli and Farouq Ali, 1984]. Brigham [1974] pointed out that the concentration of one fluid in the effluent measured during the displacement experiment was a flowing concentration (or fractional flow of the fluid as used in this study), which is different from the in-situ concentration. The definition for the flowing concentration is

$$f_s = c - \frac{D}{u}\frac{\partial c}{\partial x} . \qquad (2.2)$$

Because the gradient of concentration is negative, Equation (2.2) indicates that the average concentration flowing across a plane is always greater than the concentration in the plane. If the Neumann condition is applied at the outlet end, the flowing concentration and the in-situ concentration become identical at the outlet end.

The transition zone, as predicted by Equation (2.1), grows with the square root of time or distance travelled. If the transition zone is defined as the interval between the 10 and 90% concentrations, it can be expressed as [Walsh and Withjack, 1993]

$$\Delta L = 3.62\sqrt{\frac{\tau}{P_e}} . \qquad (2.3)$$

Equation (2.1) models successfully the performance of miscible displacements conducted in beads and sand packs [Von Rosenberg, 1956]. Zhang [1993] observed that Equation (2.1) may be valid even when the viscosity ratio is unfavorable, provided that the displacements are stable and proper effective dispersion coefficients are used.

But asymmetric effluent concentration profiles from consolidated cores, which are relatively more heterogeneous than beads or sand packs, have been observed. To explain this phenomenon, Coats and Smith [1964] proposed a capacitance model. This model includes dispersion and convection in a flowing region of the core and mass transfer between flowing and stagnant regions. By adjusting the parameters included in the model, it has been used successfully to match the skewed effluent histories of miscible displacements conducted in heterogeneous consolidated cores [Coats and Smith, 1964; Baker, 1977; Bretz and Orr, 1987]. But there is no experimental evidence to support the assumption that the stagnant volume is a physical reality. When two miscible fluids having a favorable viscosity ratio are used to conduct a displacement in a heterogeneous core, a symmetric effluent curve has been observed by Houseworth [1993]. A conclusion which may be drawn from that observation is that the capacitance effect may be a result of the permeability contrast instead of the stagnant volume.

Koval [1963] proposed a simple mathematical model for unstable miscible displacement in heterogeneous media. By assuming that mixing of the fluids can be neglected, he constructed a modified Buckley-Leverett equation, in which the permeability ratio was assumed to be proportional to the ratio of the two concentrations. One parameter was used to represent the effective viscosity ratio and another parameter was used to represent the heterogeneity of the porous medium. This model is valid only when the velocity is high enough that convection controls the process. In fact, even molecular dispersion can not be neglected at field conditions [Blackwell et al., 1959]. Koval's model predicts that a given concentration advances at a constant speed. So the transition zone length grows linearly with time. This phenomenon was observed by Walsh and Withjack [1993]

using the computer-assisted tomography (CAT) technique. But Lacey et al. [1958] pointed out that the transition zone growth was non-linear for the first few inches.

Nguyen and Bagster [1979] proposed a mathematical model for unstable miscible liquid-liquid displacement. They adopted Scheidegger's minimum energy concept to calculate the cross-sectional area of the finger zone according to the stationary point of the energy dissipation function, which is

$$A_f = \frac{1}{\mu_o/\mu_s+1} . \tag{2.4}$$

The effects of viscosity difference, density segregation and flow rate were considered in this model. But two very important factors for miscible displacement, mixing and the heterogeneity of the porous medium, were not taken into account.

As the development of new methods for in-situ concentration measurements in consolidated cores such as the CAT technique and the nuclear magnetic resonance (NMR) method [Wang et al., 1984; Hicks Jr et al., 1984; Vinegar, 1986; Hove et al., 1987] progresses, more and more evidence has appeared to support the idea that the transition zone grows linearly with time, not the square root of time as required by the standard convection-dispersion equation. To account for this phenomenon, the effective dispersion coefficient has to be scaled according to the actual field size [Pickens and Grisak, 1981]. A possible explanation for the scale dependence is that dispersion is affected by field scale heterogeneities [Hewett et al., 1993]. So, some researchers tended to use the immiscible displacement theory, which neglects the dispersion, thus emphasizing the effect that heterogeneities of the porous medium, or permeability variations, have on the linear relationship

between transition zone growth and time, in spite of the fact that dispersion in the field situation is very important.

Udey and Spanos [1991] [1993] proposed a new approach to predict miscible flood performance according to breakthrough curves obtained from the miscible displacement tests conducted on field cores. They noticed that the so-called scale-dependence of effective dispersion coefficients was a result of the "naive" application of the standard convective-dispersion equation in cases where the kinematics of the mixing zone is characterized by

$$\frac{d^2\Delta L}{dt^2} = 0, \tag{2.5}$$

which differs dramatically from that of the standard miscible theory:

$$\frac{d^2\Delta L}{dt^2} = -\frac{\sqrt{D_L}}{2t^{3/2}}. \tag{2.6}$$

Consequently, they argued that for a high flow-rate regime, the kinematics are better described by the immiscible theory than by the standard miscible theory. Udey and Spanos used a recently proposed immiscible theory and found the solution whose kinematics are consistent with experimental evidence. Unlike Koval [1963], who assumed an effective viscosity ratio, Udey and Spanos proposed that the viscosity can be related to the underlying functions $A(S_1)$ and $B(S_1)$, which appear in their solution, by

$$\frac{1}{\mu(S_1)} = \frac{A(S_1)}{\mu_1} + \frac{B(S_1)}{\mu_2}. \tag{2.7}$$

The underlying functions $A(S_1)$ and $B(S_1)$ may be computed from breakthrough curves obtained from one-dimensional field core or slim tube experiments. If the miscible displacement is conducted in a heterogeneous porous medium, the breakthrough curves are inevitably influenced by the effects of permeability variations. But it is not clear that the heterogeneities are included in the underlying function. Udey and Spanos also recognized the importance of diffusion and subjectively added this effect to their model. But no mathematical derivations were given in their paper.

Based on some observations of laboratory dispersion, measured using the CAT technique, Walsh and Withjack [1993] suggested that Fickian dispersion theory was not valid for miscible displacement in Berea sandstone. The main reason was that the Berea mixing zone growth did not grow proportional to the square root of time as required by Fickian theory; rather, it grew more nearly proportional to time. They argued that the non-Fickian flow behavior can be attributed to very small, yet significant, spatial variations in permeability. They assumed a normal (Gaussian) permeability distribution and derived a formula for concentration as follows:

$$c = \frac{1}{2}\left[1 - \operatorname{erf}\left(\frac{\xi-\tau}{\sqrt{2}V_k\tau}\right)\right] + \frac{V_k}{\sqrt{2}\pi}\exp\left[-\left(\frac{\xi-\tau}{\sqrt{2}V_k\tau}\right)^2\right] . \qquad (2.8)$$

So, the mixing zone between 3.5 and 96.5% concentrations is given by

$$\Delta L = 3.60\, V_k\tau , \qquad (2.9)$$

where V_k is a permeability variation coefficient defined by Walsh et al. [1993]. This is called the permeability variation (PV) model. But they also noticed that the PV model completely ignores the mixing contribution due to Fickian dispersion and the mixing contribution due to Fickian dispersion is largest at early times when the concentration gradient is the greatest. To improve the prediction of the mixing zone length, they assumed that the total length of the mixing zone can be approximated by adding the individual effects; that is, the total length can be computed from

$$\Delta L = 5.12 \sqrt{\frac{\tau}{P_e}} + 3.60\, V_k \tau\,. \tag{2.10}$$

This is called the permeability variation plus Fickian (PVPF) model. Equation (2.10) was used successfully to match the CAT measured transition zone growth by Walsh and Withjack. But Equation (2.8), which is based on permeability variation only, was said to be able to match the effluent curves quite well. In this case, Walsh and Withjack used the PV model to match the effluent curves and used the PVPF model to match the transition zone length data. There seems to be some doubt as to whether the Fickian dispersion should be added to the permeability variation when this approach is used to match the effluent history and the transition zone, which are important phenomena in a miscible displacement.

3. STATEMENT OF THE PROBLEM

From the survey of the literature on miscible displacement through porous media in the previous chapter, it becomes clear that the unfavorable viscosity ratio of the miscible fluids and the heterogeneity of the porous medium make the performance of a miscible displacement unpredictable by the standard convection-dispersion equation. Although immiscible theory can describe the kinematics of a miscible displacement for the late period of a process [Koval, 1963; Udey and Spanos, 1993], it can not match the transition zone growth for the early stage of the process, which takes place in a heterogeneous porous medium or in which fluids having an unfavorable viscosity ratio are used. Thus, there is a need to develop an equation which includes explicitly the viscosity ratio and the heterogeneity factor and which can be used to describe a miscible displacement adequately.

In addition to establishing a mathematical model, the second objective of this study is to find an approximate analytical solution to the proposed model to demonstrate the relationship of transition zone growth with time through an entire process.

Coskuner and Bentsen [1989] derived a dimensionless scaling group which can be used to define the boundary separating stable displacements from those which are unstable. The miscible displacements conducted in a glass bead pack by Zhang [1993] indicated that the scaling group worked well. But it is still not clear whether the heterogeneity of a porous medium affects the ease with which an instability initiates. Thus, the third objective of this study is to use linear perturbation theory, together with the proposed model, to derive a theoretical dimensionless group which can be used to predict the onset of instability of a miscible displacement conducted in a non-homogeneous porous medium.

Finally, the fourth goal is to perform some miscible displacements in a sand pack, using miscible fluids with different viscosities, to test the proposed model.

4. THEORY

The main purpose of this section is to derive a mathematical model for miscible displacement through porous media. The development of the model is based on the material balance or continuity equation and an assumption that miscible displacement may be viewed as a combination of the immiscible displacement and macroscopic dispersion of the two fluids. Darcy's law is employed to describe the immiscible displacement and the dispersion is described by Fick's law. The model may also take the properties of the fluids and the porous medium into account.

4.1 Generalized Dispersion-Convection Equation

Consider a horizontal displacement of oil by a solvent in the x direction as shown in Figure 4.1. The fluids are assumed to be miscible in all proportions. For convenience, the difference in densities of the fluids is ignored. Consequently, the effect of gravity separation may be neglected. It is also assumed that the fluids and porous medium are incompressible, and that there are no interactions between the fluids and the porous medium. Although the two fluids constitute a single phase during the course of the displacement, Darcy's law is assumed to be applicable for predicting the volumetric flow rate of each phase which is caused by the pressure gradient acting on each phase [Dougherty, 1963]. According to these assumptions, one has

$$q_{sv} = - \frac{k_s}{\mu_s} A \frac{\partial p_s}{\partial x} \qquad (4.1)$$

and

$$q_{ov} = - \frac{k_o}{\mu_o} A \frac{\partial p_o}{\partial x} . \tag{4.2}$$

The pressure in the solvent and the oil should be identical because no interface exists between the solvent and oil. The following equation must be satisfied:

$$p_s = p_o = p . \tag{4.3}$$

When two miscible fluids come in contact, mass transfer between the two fluids takes place. The mass flux is controlled by the dispersion coefficient and the concentration gradient, according to Fick's law. If the concentration of solvent is c, the concentration of the other fluid must be 1-c. When Fick's law is applied for each fluid, one has

$$q_{sD} = - D_L A \frac{\partial c}{\partial x} \tag{4.4}$$

and

$$q_{so} = - D_L A \frac{\partial (1-c)}{\partial x} . \tag{4.5}$$

The dispersion coefficient, D_L, theoretically, is concentration dependent. But generally it is treated as a constant for convenience [Perkins and Johnston, 1964].

The fluxes q_{sD} and q_{so} are equal in magnitude, but opposite in direction. The mass flux caused by concentration difference always goes from the point with higher concentration to the point with lower concentration.

In a miscible displacement, the fluids in the porous medium are subject to a pressure gradient and a concentration gradient at the same time. Auriault and Lewandowska [1994] have shown that, for chemical and water transport, the macroscopic equations reveal zero-valued cross-coupling coefficients based on passing from the micro scale to the macro scale, using the method of homogenization of periodic structures. As a consequence, the total flow rate of one fluid across any section is assumed to be a linear combination of the flow rate caused by the pressure gradient and that caused by the concentration gradient. Thus, one obtains

$$q_s = q_{sv} + q_{sD} \tag{4.6}$$

and

$$q_o = q_{ov} + q_{oD} . \tag{4.7}$$

The total flow rate of the two fluids is denoted by q and is defined by

$$q = q_s + q_o . \tag{4.8}$$

Consider a constant flow rate displacement; that is, q is constant. Now, define the fractional flow of solvent as

$$f_s = \frac{q_s}{q} . \tag{4.9}$$

Consider a small element [A (Δx) ϕ], where the concentration of solvent is c and that of oil is (1-c), at time t. The total volume of solvent is [c A (Δx) ϕ]. At the time t+Δt, the concentration of solvent increases to c+Δc. The total volume of solvent at time t+Δt must be [(c+Δc) A ϕ Δx]. During the time period Δt, the total volume of solvent flowing into the element is [$q_S(x)$ Δt], and that flowing out of the element is [$q_S(x+\Delta x)$ Δt]. From the point of view of material balance, the increase of solvent volume during time Δt must be equal to the difference of the solvent volume flowing in and flowing out of the element. That is,

$$A\phi\Delta x\Delta c = \left(- q_s(x + \Delta x) + q_s(x)\right) \Delta t . \tag{4.10}$$

Dividing the above equation by (Δx)(Δt) leads to

$$A\frac{\Delta c}{\Delta t}\phi = - \frac{q_s(x+\Delta x)-q_s(x)}{\Delta x} . \tag{4.11}$$

In the limit, as Δt and Δx approach zero, Equation (4.11) becomes

$$\frac{\partial q_s}{\partial x} + \phi A \frac{\partial c}{\partial t} = 0 . \tag{4.12}$$

Material balance is also valid for another fluid, say, oil. Thus, a similar continuity equation can be written as

$$\frac{\partial q_o}{\partial x} + \phi A \frac{\partial (1-c)}{\partial t} = 0 . \tag{4.13}$$

From Equation (4.9), q_S may be expressed as

$$q_s = q\, f_s . \tag{4.14}$$

Replacing q_S in Equation (4.12) with Equation (4.14), one has

$$q\frac{\partial f_s}{\partial x} + \phi A \frac{\partial c}{\partial t} = 0 . \tag{4.15}$$

The bulk Darcian flow rate is denoted by u and is defined as

$$u = \frac{q}{A} . \tag{4.16}$$

Thus, Equation (4.15) may be rewritten as

$$\frac{\partial f_s}{\partial x} + \frac{\phi}{u} \frac{\partial c}{\partial t} = 0 . \tag{4.17}$$

By combining Equations (4.1), (4.2), (4.3), (4.6), (4.7), (4.16), the following equation can be derived for fractional flow

$$f_s = \frac{1}{1+\frac{k_s}{k_o}\frac{\mu_o}{\mu_s}} - \frac{D_L}{u}\frac{\partial c}{\partial x} \quad . \tag{4.18}$$

By defining

$$F_s = \frac{1}{1+\frac{k_s}{k_o}\frac{\mu_o}{\mu_s}} \quad , \tag{4.19}$$

f_S can be expressed as

$$f_s = F_s - \frac{D_L}{u}\frac{\partial c}{\partial x} \quad . \tag{4.20}$$

Equation (4.20) indicates that the fractional flow of solvent, or the flowing concentration of solvent, consists of two parts. The first part, F_S, is caused by convection. The second part, $-(D_L/u)(\partial c/\partial x)$, is due to dispersion. The parameter, f_S, is always greater than F_S because $(\partial c/\partial x)$ is negative everywhere for all time.

Inserting Equation (4.20) into Equation (4.17), and considering F_S to be function of concentration only, one has

$$\frac{dF_s}{dc}\frac{\partial c}{\partial x} - \frac{D_L}{u}\frac{\partial^2 c}{\partial x^2} + \frac{\phi}{u}\frac{\partial c}{\partial t} = 0 \quad . \tag{4.21}$$

Equation (4.21) is a general convection-dispersion equation for one dimensional miscible displacement. But it is a non-linear differential equation if F_S is not linear with c.

4.2 Effective Viscosity Ratio

For immiscible displacement, viscosity ratio is defined as the ratio of the viscosity of one phase to that of the other phase. Although it has been assumed that the two miscible fluids retain their identities, with respect to their dynamic properties, when applying Darcy's law, the viscosity contrast of the two fluids is, in actual fact, moderated by dispersion. When an unfavorable viscosity ratio is considered, the effective viscosity ratio is usually taken to be some value less than that which pertains to the pure component ratio. Koval [1963] proposed a formula for effective viscosity ratio which indicates that the effective viscosity ratio is the average viscosity of a mixture of 22% solvent and 78% oil:

$$E = [0.78 + 0.22 (\frac{\mu_o}{\mu_s})^{\frac{1}{4}}]^4 . \qquad (4.22)$$

The above equation was based on a set of displacements conducted in a uniform sand pack, in which fingering and channelling were minimized. Hence, the effective viscosity, according to Koval, was isolated. In fact, the effective viscosity ratio is also affected by displacement velocity. When the velocity is slow enough for transverse diffusion to smear out the microscopic fingers, the effective viscosity ratio, which is obtained from the match calculation of experimental data using the new model derived in this chapter, is less than that calculated using Equation (4.22).

4.3 Heterogeneity Factor

When a fluid is displaced by another miscible fluid having the same viscosity as that of the displaced fluid in an absolutely homogeneous porous medium, 100% of the displaced fluid should be recovered when one pore volume of displacing fluid has been injected, if no dispersion exists. This is so called piston-like displacement, which can be achieved computationally by assuming that the effective permeability to one fluid is exactly proportional to its concentration. That is,

$$\frac{k_s}{k_o} = \frac{c}{1-c} . \tag{4.23}$$

If the porous medium is not uniform, it is inevitable that some displaced fluid will be left unrecovered when one pore volume of displacing fluid has been injected, provided the other conditions are kept unchanged [Stalkup, 1984]. This can be achieved computationally by assuming that

$$\frac{k_s}{k_o} = H\left(\frac{c}{1-c}\right) , \tag{4.24}$$

where H is a heterogeneity factor, which is greater than one. By definition, the magnitude of H is a reflection of the degree of heterogeneity of the porous medium. In fact, it is difficult to measure H directly. But it can be estimated by matching the effluent curves when two miscible fluids with equal viscosity are used.

4.4 The Function F_S

Utilizing the concepts of effective viscosity ratio, E, and heterogeneity factor, H, the function F_S of Equation (4.19) may be written as

$$F_s = \frac{c}{(1-\frac{1}{HE})\,c + \frac{1}{HE}} \quad . \tag{4.25}$$

Taking the derivative of F_S with respect to c, and putting it into Equation (4.21), one obtains

$$\frac{HE}{[(HE-1)c+1]^2}\frac{\partial c}{\partial x} - \frac{D_L}{u}\frac{\partial^2 c}{\partial x^2} + \frac{\phi}{u}\frac{\partial c}{\partial t} = 0 \, . \tag{4.26}$$

The above equation is a mathematical model which takes viscosity difference and heterogeneity into account. It is a second order non-linear partial differential equation. A numerical scheme is needed to obtain its solutions.

4.5 Dimensionless Form

To make Equation (4.26) dimensionless, the following definitions have to be introduced:

$$\tau = \frac{tu}{\phi L} \, , \tag{4.27}$$

$$\xi = \frac{x}{L} \, , \tag{4.28}$$

and

$$P_e = \frac{uL}{D_L} . \tag{4.29}$$

Then, Equation (4.26) can be rewritten as

$$\frac{HE}{[(HE-1)c+1]^2}\frac{\partial c}{\partial \xi} - \frac{1}{P_e}\frac{\partial^2 c}{\partial \xi^2} + \frac{\partial c}{\partial \tau} = 0 . \tag{4.30}$$

The concentration c is a function of ξ and τ. The entities P_e and HE may be treated as parameters.

4.6 Initial and Boundary Conditions

Consider a horizontal miscible displacement through a porous medium of length L. Initially, the medium is saturated completely with oil. Then a solvent is continuously injected at the point ξ=0. The initial condition and boundary conditions at the inlet end are as follows:

$$c(\xi, 0) = 0 \tag{4.31}$$

and

$$c(0,\tau) = 1 . \tag{4.32}$$

Next, it is assumed that the boundary condition at the outlet end takes the form [Oguztoreli and Farouq Ali, 1984]

$$\frac{\partial c}{\partial \xi}(1, \tau) = 0. \tag{4.33}$$

This assumption implies that the effect of dispersion at the outlet end is neglected, which is exactly valid before the breakthrough of the solvent. In fact, the inlet and outlet boundary conditions are important for the prediction of concentration profiles. But when the physical model becomes longer, the effect of boundary conditions for the experimental conditions employed becomes less significant [Kwok et al., 1995].

4.7 Comparison With Existing Theories

In this section, the mathematical model is compared with existing theories for simple cases. First, consider a miscible displacement in a homogeneous porous medium with fluids having the same viscosities. In that case, the effective viscosity ratio, E, and the heterogeneity factor, H, are both identically equal to one. Under these assumptions, Equation (4.30) reduces to

$$\frac{\partial c}{\partial \xi} - \frac{1}{P_e}\frac{\partial^2 c}{\partial \xi^2} + \frac{\partial c}{\partial \tau} = 0 \ . \tag{4.34}$$

The above equation is identical to the standard convection-dispersion equation. Furthermore, the fractional flow of solvent becomes

$$f_s = c - \frac{D_L}{u}\frac{\partial c}{\partial x}, \tag{4.35}$$

which is identical to the equation for flowing concentration proposed by Brigham [1974]. Second, consider another limiting case where the dispersion is neglected; that is, $D_L=0$. Then, Equation (4.20), the fractional flow equation for the solvent, becomes

$$f_s = \frac{1}{1+\frac{k_o}{k_s}\frac{\mu_s}{\mu_o}}, \tag{4.36}$$

and Equation (4.20) reduces to

$$\frac{df_s}{dc}\frac{\partial c}{\partial x} + \frac{\phi}{u}\frac{\partial c}{\partial t} = 0. \tag{4.37}$$

The solution for the above quasi-linear equation is

$$\frac{dx}{dt} = \frac{u}{\phi}\frac{df_s}{dc}. \tag{4.38}$$

The above solution is the same as the Buckley-Leverett equation for immiscible displacement, which indicates that a given concentration advances at a constant velocity, provided that df_s/dc is time-invariant.

4.8 Numerical Solution to the Proposed Model

Equation (4.30) is a non-linear, second order, partial differential equation. Exact analytical solutions to this equation are unavailable at the present time. In order to investigate the general behavior of the equation, a numerical scheme was used to find discretized solutions over the space and time domain of interest for different Peclet numbers and for different values of the product of the effective viscosity ratio and the heterogeneity factor, HE.

Numerical methods usually suffer from numerical instability problems. For Equation (4.30), the solution behavior becomes worse as the Peclet number becomes larger. Some new numerical methods have been proposed to improve the solution behavior [Oguztoreli and Farouq Ali, 1984]. But the interest here is just to find solutions of the equation. So, a finite difference approximation was utilized with cautiously selected fine grids in space ($\Delta\xi$=0.025 ~ 0.01) and small steps in time ($\Delta\tau$=1x10^{-5}~5x10^{-5}) which were chosen so that material balance requirements were satisfied to a degree of 2%. The finite difference equations were solved using the SOR method.

4.8.1 Concentration of Displacing Fluid in the Effluent

To be specific, the Peclet number was set at 400. Then, for different values of HE over the range of 1 to 10, concentrations of the displacing fluid in the effluent were calculated as a function of dimensionless time or pore volumes injected, as shown in Figure 4.2. When HE equals one, the effluent curve is very close to a symmetric "S" shape. Moreover, the breakthrough time is late, which means that a high unit displacement efficiency is to be expected. This solution is also very close to the analytical solution, which is a combination of a series of complementary error functions when the Dirichlet inlet boundary condition and

Neumann outlet boundary conditions are applied [Oguztoreli and Farouq Ali, 1984]. As HE becomes larger, the time to breakthrough becomes shorter. Also, the effluent curves no longer have the symmetric "S" shape, but become distorted and display long "tails". At a specific injected solvent volume, more displacing solvent is produced from the core via high permeability streaks or because of overriding of the more mobile injected fluid; hence, more displaced fluid is left unrecovered.

4.8.2 Transition Zone Length

Walsh and Withjack [1993] pointed out that dispersion affects both the length of the mixing zone and the effluent history. Hence, it is necessary to investigate how the mixing zone evolves with time in addition to the effluent history.

Theoretical solutions to the standard convection-diffusion equation indicate that the interval between solvent concentrations of zero and 100% is infinitely long. Therefore, the distance between 10 and 90% concentrations or other concentrations are assumed to dictate the length of the transition zone. In numerical solutions, the concentration gradients at the front and back edges of the transition zone are close to zero. It is also difficult to locate the points of zero and 100% concentration. To improve the accuracy, the interval between the 20 and 80% concentrations was defined as the transition zone length in this section.

Figure 4.3 shows the transition zone growth with dimensionless time for different combinations of the effective viscosity ratio and the heterogeneity factor, where the Peclet number was chosen, as before, as 400. For all cases, when the displacement process starts, the mixing zone grows with the square root of time, which indicates the dispersion mechanism is Fickian. But as HE increases in

magnitude and as displacement goes on, the Fickian mechanism becomes less and less significant and the transition zone grows almost linearly with time, which means that the behavior of the mixing zone growth is controlled mainly by the viscosity difference of the fluids and the heterogeneity of the porous medium.

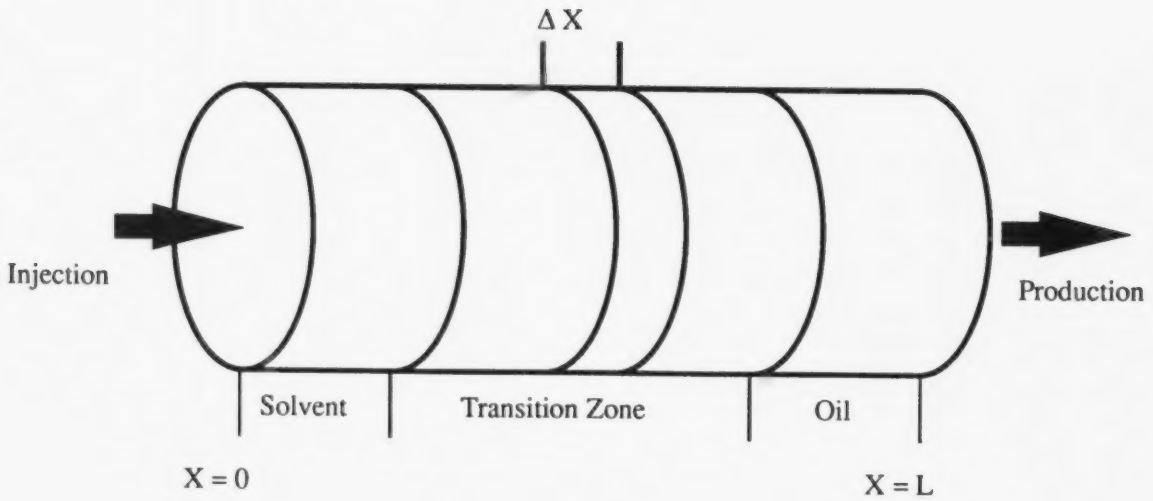

Figure 4.1 One Dimensional Porous Medium

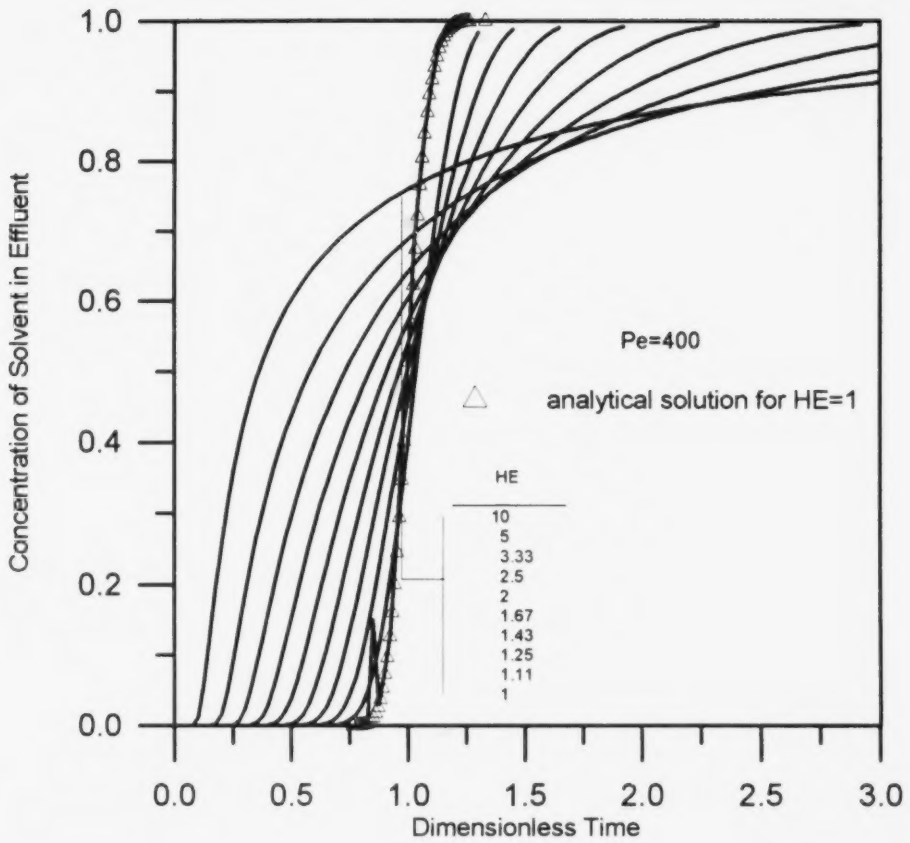

Figure 4.2 Sample Calculations of Effluent Histories Using Numerical Method

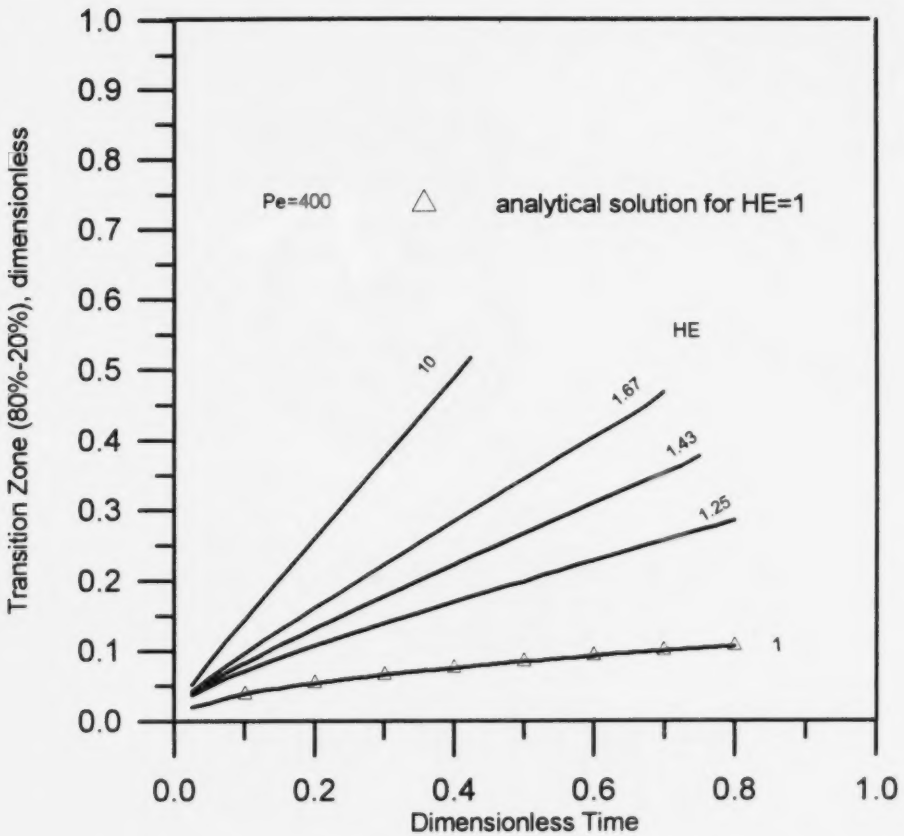

Figure 4.3 Transition Zone Length Growth from Numerical Solutions

5. APPROXIMATE ANALYTICAL SOLUTION

The purpose of this section is to demonstrate the growth of the transition zone during the course of a miscible displacement and to compare the solutions obtained from an approximate analytical scheme with those obtained from the numerical method. Because Equation (4.30) is a second-order, non-linear partial differential equation, an exact analytical solution is not available up to now, which makes it difficult to analyze the effects of some variables in the equation on the displacement performance and to avoid numerical dispersion when the convection mechanism dominates. As a consequence, even an approximate analytical solution can be very helpful in this regard.

5.1 Transition Zone Growth

The transition zone growth, in the course of a miscible displacement, is defined in this chapter as the interval between the points where the solvent concentration is 100 percent and that where the solvent concentration is zero. But in the literature, different concentration ranges have been employed because the analytical solution to the standard convection-dispersion equation indicates that the length of the transition zone between 100 percent and zero percent solvent concentration is infinite.

First, make a substitution:

$$\xi_1 = \xi - \tau . \tag{5.1}$$

Utilization of Equation (5.1) changes the solvent concentration from a function of ξ and τ to a function of ξ_1 and τ. Note that the utilization of Equation (5.1) implies that the concentration c=0.5 travels at a velocity of u/ϕ. This is valid for the standard convection-dispersion equation or when HE=1. The derivatives of c with respect to ξ and τ in terms of ξ_1 and τ can be expressed as follows:

$$\frac{\partial c}{\partial \xi} = \frac{\partial c}{\partial \xi_1}, \tag{5.2}$$

and

$$\frac{\partial^2 c}{\partial^2 \xi} = \frac{\partial^2 c}{\partial^2 \xi_1}, \tag{5.3}$$

Inserting Equations (5.2) and (5.3) into Equation (4.30), one has

$$\frac{\partial c}{\partial \tau} = \frac{1}{P_e}\frac{\partial^2 c}{\partial \xi_1^2} - \frac{HE}{[(HE-1)c+1]^2}\frac{\partial c}{\partial \xi_1}. \tag{5.4}$$

Use is made now of the transformation

$$\eta = \frac{\xi_1}{\lambda(\tau)}, \tag{5.5}$$

where $\lambda(\tau)$ is the half length of the transition zone, which is a function only of time. Utilizing this transformation, the dimensionless length η is scaled by the transition

zone length between -1 and 1. To proceed further, it is necessary to assume a function for $c(\eta)$. It is convenient to use the following polynomial form:

$$c = \frac{1}{4}(\eta^3 - 3\eta + 2) . \tag{5.6}$$

Note that, other functional forms for $c(\eta)$, such as higher order polynomials, or even the error function, could have been used. However, Equation (5.6) was selected because of its simplicity. The accuracy of the assumed concentration profile depends on how far away it is from the real concentration distribution, which is unknown. But it is thought that these kinds of curves are similar to the real concentration profile, and it is known that they satisfy the following boundary conditions:

$$c(-1) = 1 , \tag{5.7}$$

and

$$c(1) = 0 . \tag{5.8}$$

The derivatives of $c(\eta)$ with respect to η are as follows:

$$\frac{\partial c}{\partial \eta} = \frac{3}{4}(\eta^2 - 1) , \tag{5.9}$$

and

$$\frac{\partial^2 c}{\partial \eta^2} = \frac{3}{2}\eta \,. \tag{5.10}$$

The first and second order derivatives of the concentration, c, with respect to ξ_1 are obtained through Equations (5.9) and (5.10). They may be written as

$$\frac{\partial c}{\partial \xi_1} = \frac{1}{\lambda(\tau)}\frac{\partial c}{\partial \eta}\,, \tag{5.11}$$

and

$$\frac{\partial^2 c}{\partial \xi_1^2} = \frac{1}{\lambda(\tau)^2}\frac{\partial^2 c}{\partial \eta^2}\,. \tag{5.12}$$

Multiplying Equation (5.4) by η and integrating the resulting equation over the range of η from -1 to 1 lead to

$$\int_{-1}^{1}\frac{\partial c}{\partial \tau}\eta d\eta = \int_{-1}^{1}\frac{1}{P_e}\frac{\partial^2 c}{\partial \xi_1^2}\eta d\eta - \int_{-1}^{1}\frac{HE}{[(HE-1)c+1]^2}\frac{\partial c}{\partial \xi_1}\eta d\eta\,. \tag{5.13}$$

Inserting Equations (5.9) through (5.12) into Equation (5.13), and completing the integration, one has

$$\lambda\frac{d\lambda}{d\tau} = \frac{5}{P_e} + \frac{15}{4}I_o\lambda\,, \tag{5.14}$$

where

$$I_o = \int_{-1}^{1} \frac{HE}{[(HE-1)c+1]^2} (1-\eta^2)\eta d\eta \ . \tag{5.15}$$

The integral I_O reflects the effect of heterogeneity and viscosity ratio. When the product of HE is one, I_O is zero. When HE increases, I_O also increases, as shown in Figure 5.1.

Now, consider two limiting conditions:

1). When τ approaches zero, the half transition zone length, $\lambda(\tau)$, must also be very small. In this case, $\lambda(\tau)$ is assumed to be negligible. Then, Equation (5.14) may be simplified to

$$\lambda \frac{d\lambda}{d\tau} = \frac{5}{P_e} \ . \tag{5.16}$$

The solution to Equation (5.16), with initial condition of $\lambda(0)=0$, is

$$\lambda(\tau) = \sqrt{\frac{10}{P_e}\tau} \ . \tag{5.17}$$

In order to compare the transition zone length predicted using Equation (5.17) with that obtained using the standard convection-dispersion equation, Equation (5.17) has be converted into the transition zone length between concentrations of 3.5 and 96.5%. According to Equation (5.6), the transition zone length between the concentrations of 3.5 and 96.5% is about 77.3% of $2\lambda(\tau)$. Consequently,

$$\lambda_{3.5\%-96.5\%} \cong 4.90 \sqrt{\frac{\tau}{P_e}} \,. \tag{5.18}$$

The transition zone length, obtained using the same concentration range calculated from the standard convection-diffusion equation, has the same form as Equation (5.18). But the coefficient preceeding the square root sign is 5.12. The coefficient in Equation (5.18) changes slightly with different assumed functions for $c(\eta)$. The fact that Equation (5.18) is similar to that which is derived using the standard convection-diffusion equation suggests that the miscible displacement process, during the early stage, is controlled mainly by the Fickian dispersion mechanism.

2). When τ approaches infinity, the second term on the right hand side of Equation (5.14) must be much greater than the first one. In this case, it may be neglected; that is,

$$\frac{d\lambda}{d\tau} = \frac{15}{4} I_o \,. \tag{5.19}$$

Under these conditions, Equation (5.19) can be integrated to obtain

$$\lambda(\tau) = \frac{15}{4} I_o \tau \,. \tag{5.20}$$

Obviously, $\lambda(\tau)$ increases linearly with dimensionless time τ. The transition zone length between the 3.5% and 96.5% concentrations can also be shown to be defined by

$$\lambda_{3.5\%-96.5\%} \cong 5.80 \, I_o \tau \,. \tag{5.21}$$

Walsh and Withjack [1993] derived the following formula for the transition zone length from his permeability-variation model:

$$\lambda_{3.5\%\text{-}96.5\%} = 3.6\ V_k\ \tau\ , \tag{5.22}$$

where V_k is the coefficient of permeability variation. It is very clear that equations (5.21) and (5.22) both indicate that the transition zone length grows linearly with time. Although I_o and V_k serve the same purpose, they may have different forms. Consequently, the two equations have different coefficients. In fact, Walsh and Withjack [1993] added a second term which resulted from the inclusion of Fickian dispersion in his formula:

$$\lambda_{3.5\%\text{-}96.5\%} = 3.6\ V_k\tau + 5.12\sqrt{\frac{\tau}{P_e}}\ . \tag{5.23}$$

Note that the second term continues to grow with time, although he reasoned that the Fickian dispersion should die out as the flood front advances away from the inlet end.

Equation (5.14) can be integrated to yield

$$\tau = \frac{\lambda}{a} - \frac{b}{a^2}\ln\left(\frac{a\lambda+b}{b}\right)\ , \tag{5.24}$$

where

$$a = \frac{15}{4}\ I_o\ , \tag{5.25}$$

and

$$b = \frac{5}{P_e} . \tag{5.26}$$

Note that Equation (5.14) can be rewritten as the following form:

$$\frac{d\lambda}{d\tau} = \frac{15}{4} I_o + \frac{5}{P_e \lambda} . \tag{5.27}$$

If the second term on the right hand side of Equation (5.27) approaches zero, the derivative of λ with respect to τ will be close to a constant, $(15/4)I_O$, which means that the transition zone grows linearly with time, hence dictating a non-Fickian-dominated mechanism. With a larger Peclet number, i.e. smaller dispersion coefficient, and a longer transition zone length, i.e. later times of a miscible displacement, the second term is closer to zero. Figure 5.2 presents the half lengths of the mixing zone obtained using Equation (5.24). For the two cases where HE is 1.5 and 2, respectively, the Fickian dispersion mechanism dominates during the early time. As a displacement goes on, the heterogeneity of a porous medium and the viscosity difference of the two fluids control the behavior of the transition zone growth.

5.2 Procedure for Calculating f_S

In this section, the procedure used to calculate the effluent history curves for a one-dimensional miscible displacement based on the approximate solution scheme are discussed. Then the solution is compared with that obtained using the numerical method.

At the outlet end, ξ equals one. It is desired to calculate the fractional flow of the solvent, f_S, at dimensionless time, τ. The procedure for doing this is outlined below.

1) calculate the half length of the mixing zone length, λ, according to Equation (5.24);

2) calculate the variable η from

$$\eta = \frac{1-\tau}{\lambda}, \qquad (-1 \le \eta \le 1); \tag{5.28}$$

3) calculate the concentration at ξ=1, according to Equation (5.6). But note that c is one when η is less than -1 and is zero when η is greater than 1;

4) calculate f_S using

$$f_s = \frac{c}{(1-\frac{1}{HE})c + \frac{1}{HE}} + \frac{3}{4}\frac{(1-\eta^2)}{P_e\lambda}. \tag{5.29}$$

The above steps are based on the assumption that, after breakthrough of the injected solvent, the "S" shaped concentration profiles are assumed to proceed along the x direction continuously. In this case, the derivative of the concentration c with respect to distance x at the outlet end is no longer zero, which yields the second term on the right hand side of Equation (5.29).

5.3 Comparison with Numerical Solution

Figures 5.3 through 5.5 show comparisons of effluent curves obtained using the numerical and approximate schemes. According to the analytical solution to the mathematical model (Equation 4.30) with HE=1, the concentration distribution at a given time is a combination of error functions, which takes a symmetric "S" shape approximately [Oguztoreli, M. and Farouq Ali, 1984]. In the approximate analytical scheme, the concentration profiles are assumed to take a symmetric "S" shape (approximated by a third degree polynomial) for all cases. Consequently, a very good agreement is achieved for the case of HE=1, as shown in Figure 5.3. Only for the breakthrough time and the time when the solvent concentration in the effluent approaches 1, is the difference in the two solutions detectable, which arises out of the difference in the assumed and the true concentration profiles. Figure 5.4 shows the comparison of the effluent curves when HE equals 1.25, indicating also a good agreement. As HE becomes more removed from 1 and the standard miscible theory does not apply, the true concentration profiles are distorted. But in the approximate analytical solution scheme, the concentration profiles are assumed to have the same shape. As a consequence, the accuracy of the solution using the approximate analytical scheme

decreases. As shown in Figure 5.5 for HE=2, the difference between the solvent concentrations in the effluent predicted using the approximate method and the numerical scheme is pronounced, but still acceptable.

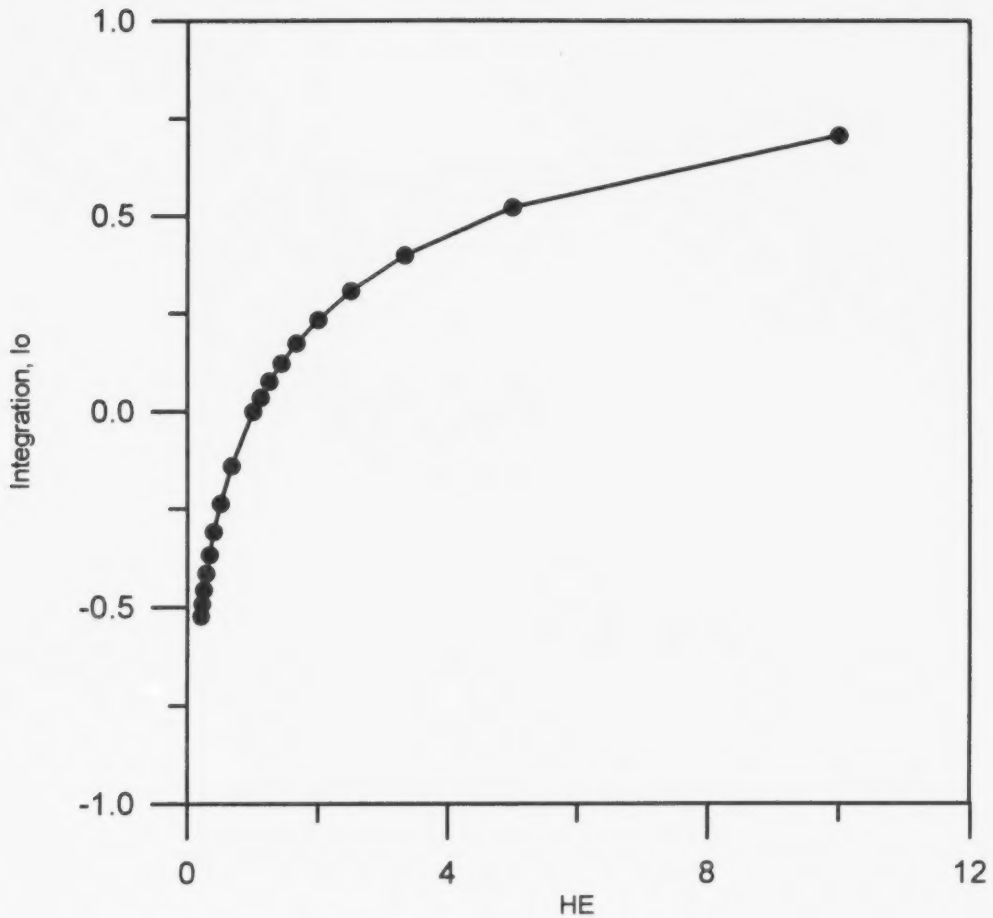

Figure 5.1 Integration of Equation (5.17) versus HE

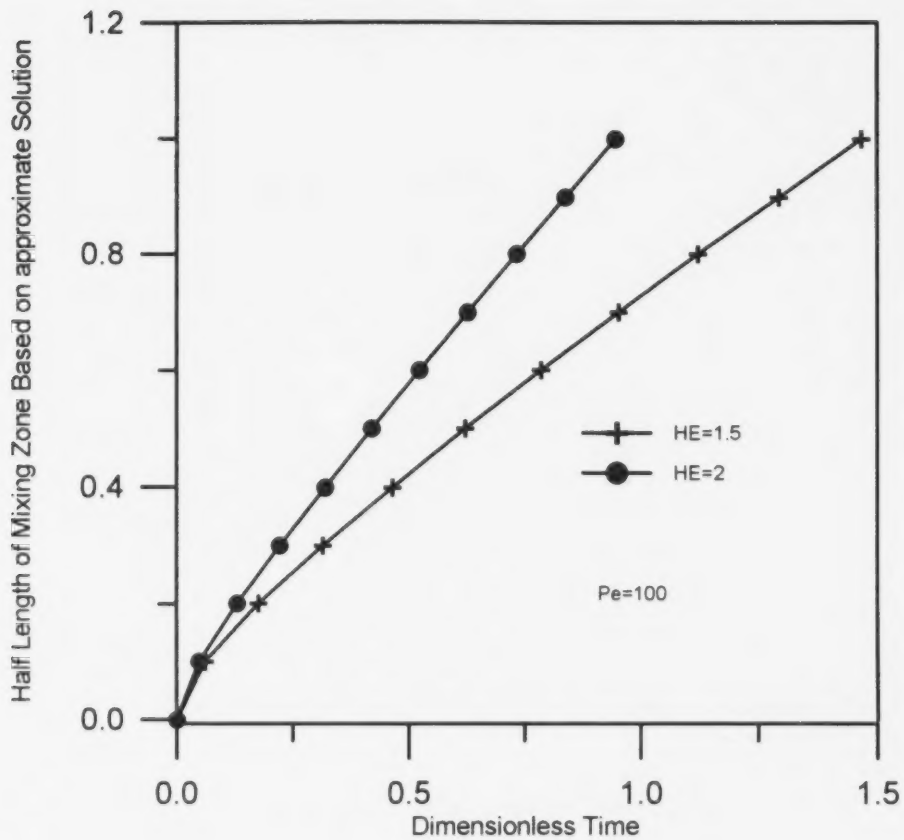

Figure 5.2 Half Transition Zone Length Growth Using Approximate Analytical Scheme

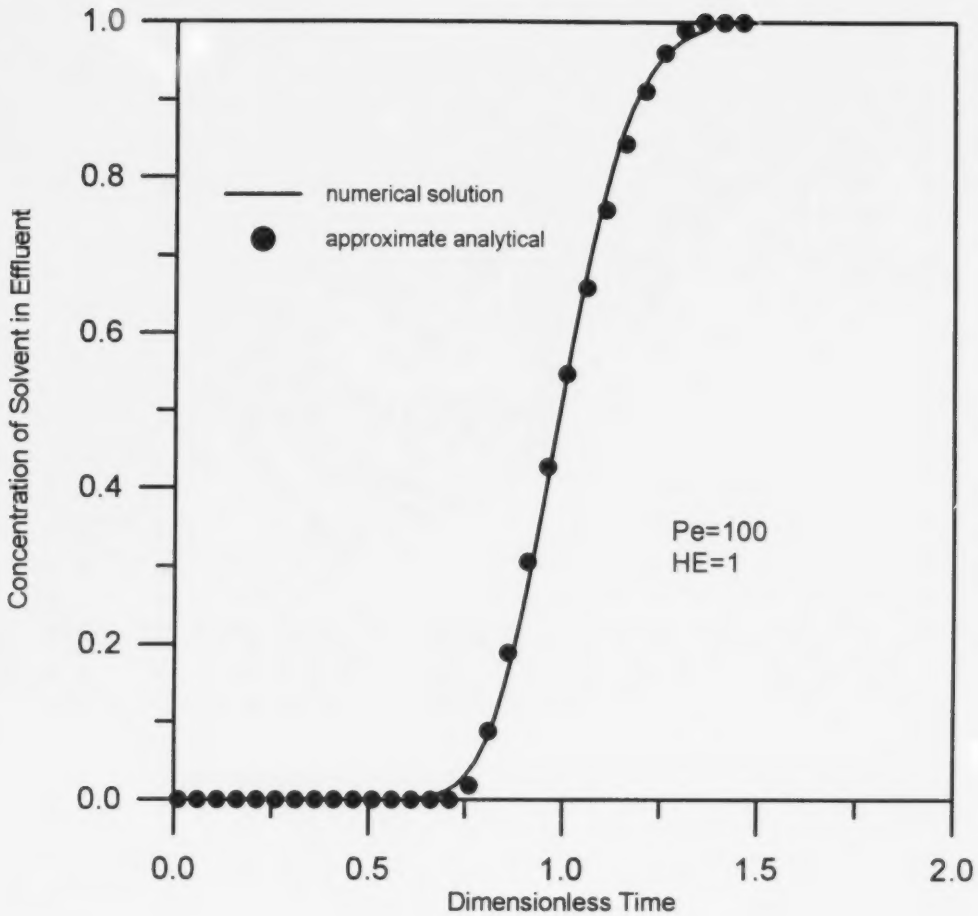

Figure 5.3 Effluent History Using Numerical and Approximate Schemes (HE=1)

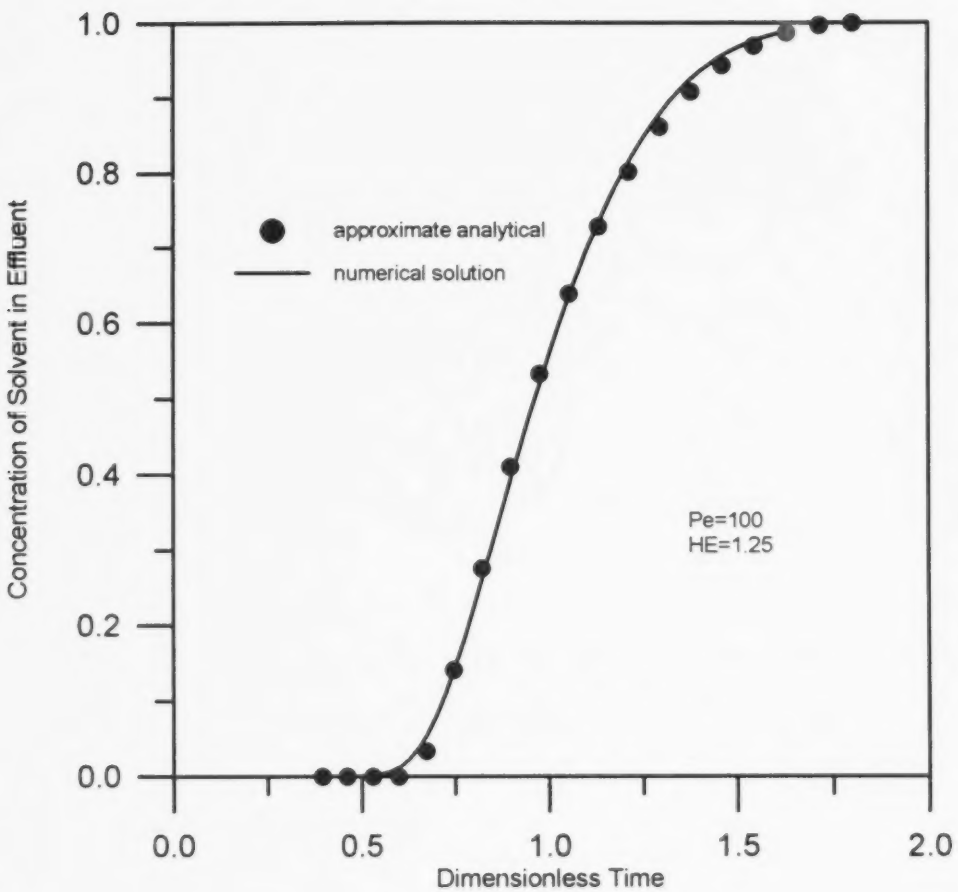

Figure 5.4 Effluent History Using Numerical and Approximate Schemes (HE=1.25)

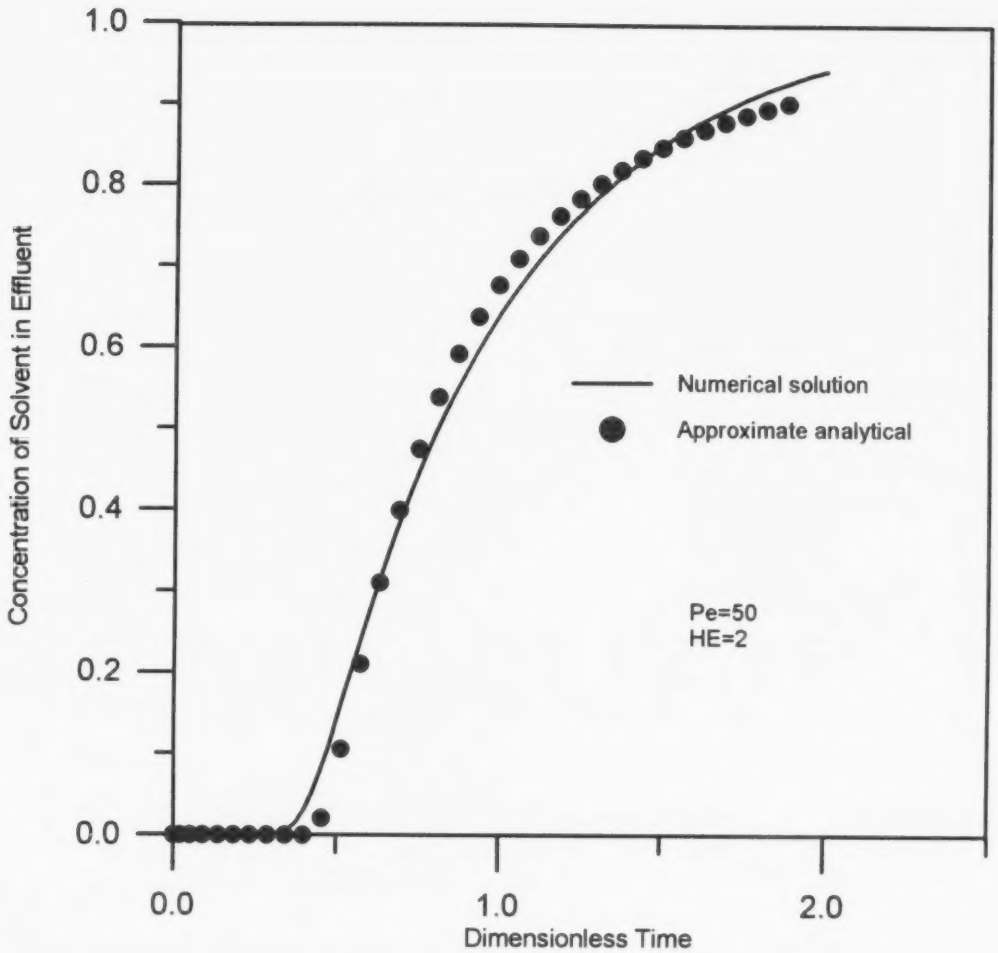

Figure 5.5 Effluent History Using Numerical and Approximate Schemes (HE=2)

6. COMPARISONS WITH PUBLISHED DATA

In this section, numerical solutions to Equation (4.30) and the approximate analytical solutions to Equation (4.30) (derived in chapter 5) are used to match some published experimental data by adjusting the product of the effective viscosity ratio and the heterogeneity factor, HE, as well as the Peclet number. The parameters which prevent the standard convection-diffusion equation from describing a real miscible displacement process properly are the difference of viscosities of the fluids and the heterogeneity of the porous medium. Hence, two kinds of miscible flooding data were chosen to be compared with the solutions to Equation (4.30). The first kind involves miscible displacements using fluids with different viscosities, but conducted in uniform porous media, such as a sand pack. The second type involves miscible displacements conducted in a consolidated sandstone, such as a Berea core, which is considered to be heterogeneous.

6.1 Comparison with Brigham et al.'s Data

Brigham et al. [1961] reported a series of experiments on miscible displacements in various porous media. In studying the effect of viscosity ratio on the mixing process, they performed an unstable miscible displacement with a pair of oils for which the viscosity ratio of the displaced to displacing oil was 5.71. The experiment was performed in a glass-bead pack with an average bead diameter of 0.1 mm. They observed the development and growth of viscous fingers. Their experimental results for this case are matched using the newly developed

mathematical model, Equation (4.30). The porous medium, glass-bead pack, is considered to be uniform. As a consequence, the heterogeneity factor, H, is believed to be 1. To match the experimental data, the effective viscosity ratio and the Peclet number are adjusted to be 1.33 and 50, respectively. The effective viscosity ratio matched here is slightly smaller than 1.57, which is calculated using Koval's formula. Figure 6.1 shows concentrations of the displacing fluid in the effluent for both the experimental and the model results. In view of the disturbances in the experimental data, the agreement is reasonably good.

6.2 Comparison with Withjack's Data

Withjack [1988] performed two miscible displacements using fluids with viscosity ratios of 0.97:1 and 67:1, respectively. The displacements were conducted in a Berea consolidated core, which is not as homogeneous as a glass-bead pack. In addition to the concentrations of displacing fluid in the effluent, measured with time, the normalized distance, which was defined by Withjack as the dimensionless flood front position, was also determined at the same time by use of the CAT technique. Their results were matched also using the new model in such a way that, using one set of optimal HE and Peclet numbers, the effluent histories and the normalized distances were matched simultaneously. Figures 6.2 and 6.3 compare the experimentally determined and calculated, using the approximate analytical solution, effluent curves and the normalized distance curves, for the 0.97:1 and 67:1 viscosity ratio curves, respectively. While the agreement for the 0.97:1 viscosity case is good, the 67:1 viscosity ratio case is less satisfactory. For the first

case, the matched HE and P_e are 1.05 and 200, respectively. Consequently, the approximate analytical scheme works quite well in this range of HE and P_e. The good agreement is probably due to the slightly favorable viscosity ratio. For the second case, the matched HE and P_e are around 4.3 and 7, respectively. As demonstrated in Chapter 5, the difference between the assumed symmetric concentration profiles and the distorted ones may be the reason for the pronounced difference between the experimental and matched data.

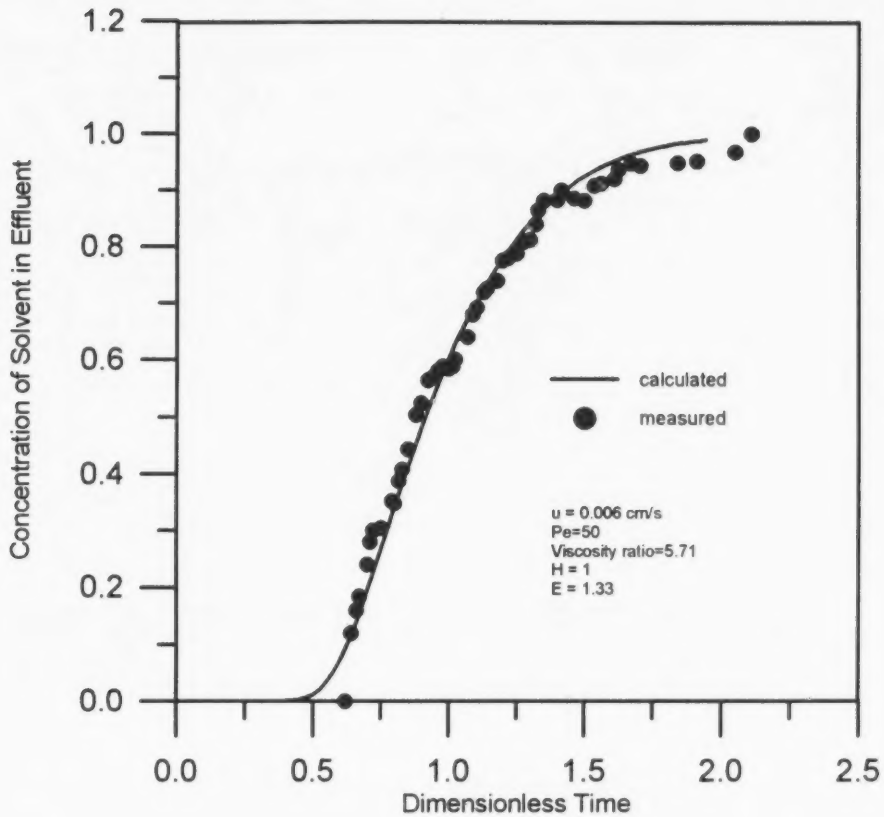

Figure 6.1 Comparison of Effluent Curve of Brigham's Data with Numerical Solution

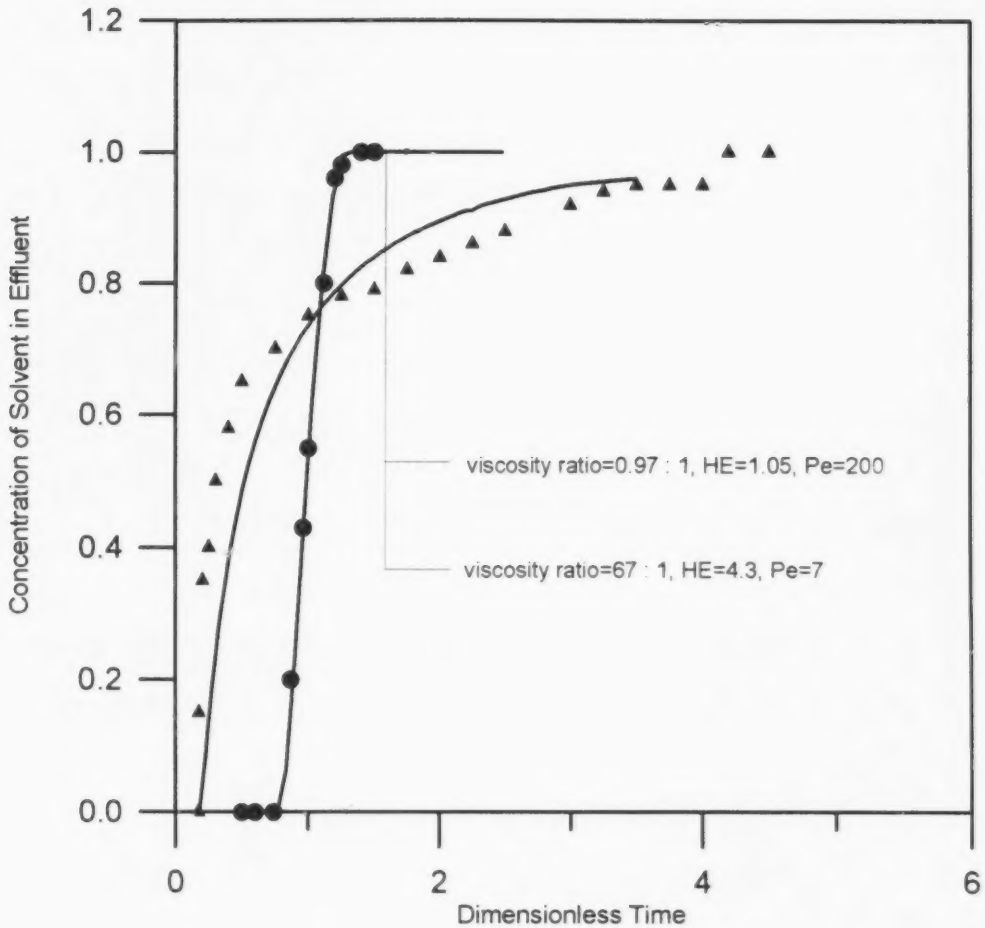

Figure 6.2 Comparison of Effluent Curves of Withjack's Data with Approximate Analytical Solution

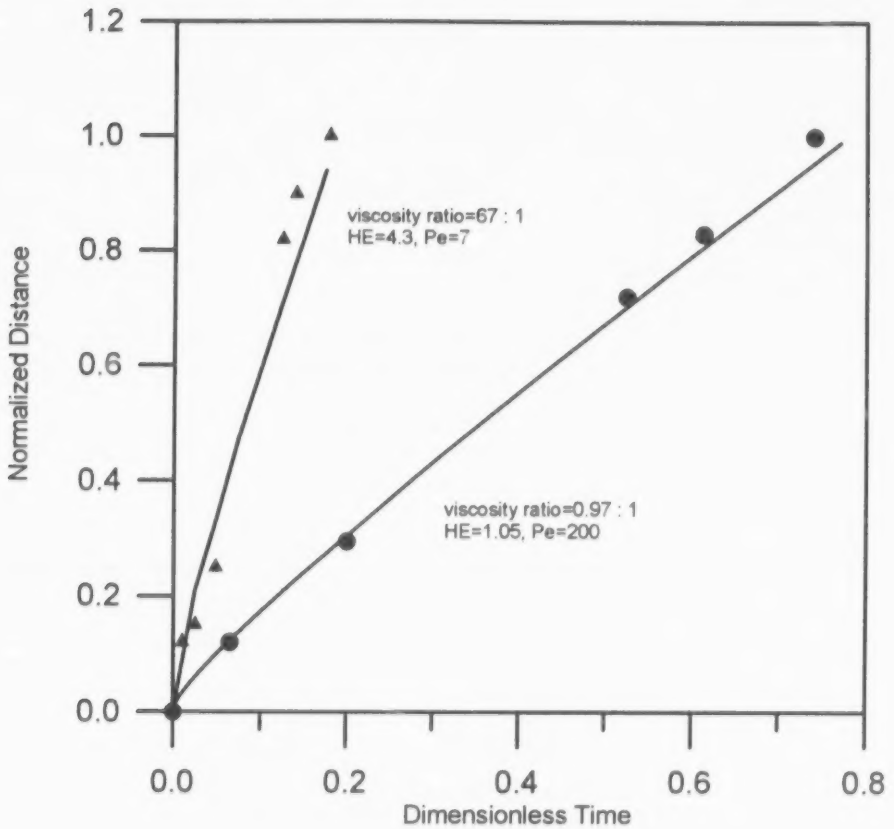

Figure 6.3 Comparison of Normalized Distance of Withjack's Data with Approximate Analytical Solution

7. PREDICTION OF THE ONSET OF INSTABILITY

Coskuner and Bentsen [1989] derived a dimensionless scaling group to predict the onset of instability for miscible displacement based on small perturbation theory . In their derivations, the standard convection-dispersion equation, which is valid for matched fluids and homogeneous porous media, was used. Their scaling group has been tested by Zhang's [1993] miscible displacements conducted in glass-bead pack porous media. Although it has been recognized that, even a very small heterogeneity of the porous medium, such as permeability variation, may initiate instability, it is not clear if the degree of the heterogeneity of a porous medium has any effect on the ease with which an instability initiates.

In this chapter, some theoretical analysis is undertaken on how heterogeneity affects the onset of instability. This analysis is based on linear perturbation theory, together with the newly proposed mathematical model derived in Chapter 4. The miscible displacements in a homogeneous porous medium conducted in this study showed that the effective viscosity ratio approaches one when displacement velocities are very small or when the displacements are stable. Hence, in this chapter, the effective viscosity ratio is assumed to be one because what is considered here is the onset of an instability.

7.1 Basic Equations

Consider a downward displacement of one fluid by another in the z' direction in a heterogeneous porous medium (H>1) as shown in Figure 7.1. The mathematical description of the flow system is given by [Neuman, 1977]

$$\frac{\partial u}{\partial x}+\frac{\partial v}{\partial y}+\frac{\partial w}{\partial z'}=0, \tag{7.1}$$

$$\frac{\rho}{\phi}\frac{\partial u}{\partial t}+\frac{\partial p}{\partial x}+\frac{\mu}{k}u=0, \tag{7.2}$$

$$\frac{\rho}{\phi}\frac{\partial v}{\partial t}+\frac{\partial p}{\partial y}+\frac{\mu}{k}v=0, \tag{7.3}$$

$$\frac{\rho}{\phi}\frac{\partial w}{\partial t}+\frac{\partial p}{\partial z'}+\frac{\mu}{k}w-\rho g=0, \tag{7.4}$$

and

$$\frac{\partial c}{\partial t}+\frac{u}{\phi}\frac{\partial c}{\partial x}+\frac{v}{\phi}\frac{\partial c}{\partial y}+\frac{w}{\phi}\psi(c)\frac{\partial c}{\partial z'}-D_T\left(\frac{\partial^2 c}{\partial x^2}+\frac{\partial^2 c}{\partial y^2}\right)-D_L\frac{\partial^2 c}{\partial z'^2}=0, \tag{7.5}$$

where

$$\psi(c)=\frac{H}{[(H-1)c+1]^2}. \tag{7.6}$$

When the displacement is stable, one has

$$\bar{u}=\bar{v}=0, \tag{7.7}$$

$$\bar{w}=V=0, \tag{7.8}$$

$$\frac{\partial \bar{p}}{\partial x} = \frac{\partial \bar{p}}{\partial y} = 0 \,, \tag{7.9}$$

$$\frac{\partial \bar{p}}{\partial z'} + \frac{\mu}{k} V - \bar{\rho}\, g = 0 \,, \tag{7.10}$$

and

$$\frac{\partial \bar{c}}{\partial t} + \frac{V}{\phi} \psi(\bar{c}) \frac{\partial \bar{c}}{\partial z'} - D_L \frac{\partial^2 \bar{c}}{\partial z'^2} = 0 \,. \tag{7.11}$$

7.2 Small Perturbations Theory

According to the small perturbation scheme, the dependent variables of a system are slightly disturbed about their stable values to examine the stability of the disturbed variables. Thus,

$$\zeta = \bar{\zeta} + \zeta^* \,, \tag{7.12}$$

where

$$\zeta = c, u, v, w, p, \rho, \mu \,. \tag{7.12a}$$

Then, Equation (7.12) is inserted into Equations (7.7) through (7.11). If the non-linear terms are neglected in the resulting equations, the following set of linear

partial differential equations, in the moving coordinates given by $z=z'-vt/\phi$, are obtained:

$$\frac{\partial u^*}{\partial x} + \frac{\partial v^*}{\partial y} + \frac{\partial w^*}{\partial z} = 0 , \tag{7.13}$$

$$\frac{\rho}{\phi}\frac{\partial u^*}{\partial t} + \frac{\partial p^*}{\partial x} + \frac{\bar{\mu}}{k}u^* = 0 , \tag{7.14}$$

$$\frac{\rho}{\phi}\frac{\partial v^*}{\partial t} + \frac{\partial p^*}{\partial y} + \frac{\bar{\mu}}{k}v^* = 0 , \tag{7.15}$$

$$\frac{\rho}{\phi}\frac{\partial w^*}{\partial t} + \frac{\partial p^*}{\partial z} + \frac{\bar{\mu}}{k}w^* + \frac{V}{k}\frac{d\mu}{dc}c^* - \frac{d\rho}{dc}c^* g = 0 , \tag{7.16}$$

and

$$\frac{\partial c^*}{\partial t} + \frac{V}{\phi}\psi(\bar{c})\frac{\partial c^*}{\partial z} + \left[\frac{V}{\phi}\frac{d\psi}{dc}c^* + \psi(\bar{c})\right]\frac{\partial \bar{c}}{\partial z} - D_T\left(\frac{\partial^2 c^*}{\partial x^2} + \frac{\partial^2 c^*}{\partial y^2}\right)$$

$$- D_L\frac{\partial^2 c^*}{\partial z^2} = 0 \tag{7.17}$$

A disturbance in a linear system may be expressed as a Fourier series. Therefore,

$$\zeta^* = \tilde{\zeta}(z)\, e^{i(\alpha x + \beta y) + \sigma t} . \tag{7.18}$$

If an appropriate form of Equation (7.18) is substituted into Equations (7.13) to (7.17), the perturbation variables $\tilde{u}(z)$, $\tilde{v}(z)$ and $\tilde{p}(z)$ may be eliminated. Two ordinary differential equations coupling $\tilde{c}(z)$ and $\tilde{w}(z)$ are obtained:

$$[-(\frac{\rho\sigma}{\phi\gamma} + \frac{\bar{\mu}}{k\gamma^2}) D^2 - (\frac{\sigma}{\phi\gamma^2}\frac{d\bar{\rho}}{dz} + \frac{1}{k\gamma^2}\frac{d\bar{\mu}}{dz}) D + (\frac{\bar{\mu}}{k} + \frac{\overline{\rho\,\sigma}}{\phi})]\ \tilde{w} = - N_C\ \tilde{c}(z)\ , \tag{7.19}$$

and

$$[D^2 - \frac{D_T}{D_L}\gamma^2 - \frac{V}{\phi D_L}\frac{d\psi}{dc}\frac{\partial\bar{c}}{\partial z} - \frac{\sigma}{D_L}]\ \tilde{c}(z) = \frac{\psi(\bar{c})}{D_L\phi}\frac{\partial\bar{c}}{\partial z}\ \tilde{w}(z)\ , \tag{7.20}$$

where

$$N_C = \frac{V}{k}\frac{d\mu}{dc} - \frac{d\rho}{dc}\,g\ , \tag{7.21}$$

and

$$\gamma^2 = \alpha^2 + \beta^2\ . \tag{7.22}$$

The operator, D, represents differentiation with respect to the z direction.

7.3 Marginal Instability

Coskuner and Bentsen [1989] pointed out that the marginal state is characterized by $\sigma = 0$. If advantage is taken of this fact, Equations (7.19) and (7.20) may be simplified as

$$[\, D^2 + M\, D - \gamma^2] = \frac{N_c k \gamma^2}{\bar{\mu}}\, \tilde{c}(z)\,, \tag{7.23}$$

and

$$[D^2 - K\,\gamma^2 - \frac{V}{\phi D_L}\frac{d\psi}{dc}\frac{\partial \bar{c}}{\partial z}\,]\,\tilde{c}(z) = \frac{\psi(\bar{c})}{D_L \phi}\frac{\partial \bar{c}}{\partial z}\,\tilde{w}(z)\,, \tag{7.24}$$

where

$$M = \frac{d\,\ln\bar{\mu}}{dz}\,, \tag{7.25}$$

and

$$K = \frac{D_T}{D_L}\,. \tag{7.26}$$

Coskuner and Bentsen [1989] reasoned that any arbitrary small perturbation which grows or decays within the very small time period after time zero will continue to do so for the whole duration of the displacement. As a consequence, it is assumed that $\partial c^*/\partial z$ is negligible for times only slightly larger than zero [Coskuner, 1987]. And the boundary conditions for Equations (7.23) and (7.24) are as follows:

$$\tilde{c}(z) = 0 \quad \text{at } z = 0 \text{ and } z = L, \tag{7.27}$$

and

$$\tilde{w}(z) = 0 \quad \text{at } z = 0 \text{ and } z = L. \tag{7.28}$$

Equations (7.23) and (7.24), together with boundary conditions (7.28) and (7.29), may be solved using a variational scheme, which has been used in the stability analysis of natural convection [Chandrasekhar, 1961]. Hence, it is assumed that $\tilde{w}(z)$ can be expressed in the form of a sine series:

$$\tilde{w}(z) = \sum_{m=1}^{\infty} A_m \sin\left(\frac{m\pi z}{L}\right). \tag{7.29}$$

Inserting Equation (7.29) into (7.24) yields

$$\left(D^2 - K\gamma - \frac{V}{\phi D_L}\frac{d\psi}{dc}\frac{\partial \bar{c}}{\partial z}\right)\tilde{c}(z) = \frac{\psi(\bar{c})}{D_L\phi}\frac{\partial \bar{c}}{\partial z}\sum_{m=1}^{\infty} A_m \sin\left(\frac{m\pi z}{L}\right). \tag{7.30}$$

Because Equation (7.30) is a linear, ordinary differential equation, the solution $\tilde{c}(z)$ may be assumed to take the form

$$\tilde{c}(z) = \frac{\psi(\bar{c})}{D_L\phi}\frac{\partial \bar{c}}{\partial z}\sum_{m=1}^{\infty} A_m C_m, \tag{7.31}$$

where $C_m(z)$ is the solution of the equation

$$(D^2 - K\gamma^2 - \frac{V}{D_L\phi}\frac{d\psi}{dc}\frac{\partial \bar{c}}{\partial z})\, C_m = \sin(\frac{m\pi z}{L}) , \tag{7.32}$$

which satisfies the following boundary conditions:

$$C_m(0) = 0 , \tag{7.33}$$

and

$$C_m(L) = 0 . \tag{7.34}$$

Putting the assumed solutions of $\tilde{c}(z)$ and $\tilde{w}(z)$ into Equation (7.23) leads to

$$(D^2 + MD - \gamma^2) \sum_{m=1}^{\infty} A_m \sin(\frac{m\pi z}{L}) = \frac{N_c k\gamma^2 \psi(\bar{c})}{\bar{\mu}\phi D_L}\frac{\partial \bar{c}}{\partial z} \sum_{m=1}^{\infty} A_m C_m(z) . \tag{7.35}$$

Undertaking the differentiations, one has

$$\sum_{m=1}^{\infty} A_m\gamma_m \sin(\frac{m\pi z}{L}) - \sum_{m=1}^{\infty} A_m\beta_m \cos(\frac{m\pi z}{L}) = R^2\gamma^2 \sum_{m=1}^{\infty} A_m C_m(z) , \tag{7.36}$$

where

$$R^2 = -\frac{kN_c\psi(\bar{c})}{\bar{\mu}\phi D_L}\frac{\partial \bar{c}}{\partial z}\,, \tag{7.37}$$

$$\gamma_m = \left(\frac{m\pi}{L}\right)^2 + \gamma^2\,, \tag{7.38}$$

and

$$\beta_m = \frac{Mm\pi}{L} \tag{7.39}$$

Multiplying Equation (7.36) with $\sin(n\pi z/L)$ (n=1, 2, ...), and integrating it with respect to z over the range of 0 to L, one obtains

$$\sum_{m=1}^{\infty}\left[\frac{\delta_{mn}\gamma_m L}{2R^2\gamma} - \frac{2n\beta L}{\pi R^2\gamma^2(n^2-m^2)} - \int_0^L C_m(z)\sin\left(\frac{n\pi z}{L}\right)dz\right]A_m = 0\,,$$

$$n=1,\ 2,\ \ldots \tag{7.40}$$

where,

δ_{mn} = 1 only when n=m; otherwise, it is zero.

The second term in Equation (7.40) should be set equal to zero when (n-m) is even. From Equations (7.32) through (7.34), C_m can be solved for as

$$C_m(z) = -\frac{\sin\left(\frac{m\pi z}{L}\right)}{\frac{m^2\pi^2}{L^2} + K\gamma^2 + \frac{V}{\phi D_L}\frac{d\psi}{dc}\frac{\partial \bar{c}}{\partial z}}\,, \tag{7.41}$$

provided that $\partial\bar{c}/\partial z$ is considered an average concentration gradient over the life of a displacement [Coskuner and Bentsen, 1989]. Then,

$$\int_0^L C_m(z)\sin(\frac{n\pi z}{L})dz = -\frac{\delta_{mn}L}{2(\frac{m^2\pi^2}{L^2} + K\gamma^2 + \frac{V}{\phi D_L}\frac{d\psi}{dc}\frac{\partial\bar{c}}{\partial z})} . \tag{7.42}$$

Because Equation (7.40) represents a system of homogeneous, linear equations for A_m, it is necessary for the determinant of the coefficient matrix to be zero in order that A_m has non-trival solutions. That is,

$$\det(\frac{\delta_{mn}\gamma_m L}{2R^2\gamma^2} - \frac{2n\beta_m L}{\pi R^2\gamma^2(n^2-m^2)} + \frac{\delta_{mn}L}{(\frac{m^2\pi^2}{L^2} + K\gamma^2 + \frac{V}{\phi D_L}\frac{d\psi}{dc}\frac{\partial\bar{c}}{\partial z})}) = 0 ,$$

$$m=1, 2, ..., n=1, 2, ... \tag{7.43}$$

The actual condition for marginal instability can be obtained by solving Equation (7.43). Chandrasekhar [1961] has shown that even the vanishing of the upper left element of the determinant yields a very good approximation to the exact condition of marginal instability in natural convection. Then, following Chandrasekhar's analysis gives

$$\frac{L\gamma_{m=1}}{2R^2\gamma^2} + \frac{L}{2(\frac{\pi^2}{L^2} + K\gamma^2 + \frac{V}{\phi D_L}\frac{d\psi}{dc}\frac{\partial\bar{c}}{\partial z})} = 0 . \tag{7.44}$$

Inserting the expression for $\gamma_{m=1}$ and R^2 into Equation (7.44), one obtains

$$\left[\frac{kN_c\psi(\bar{c})}{\bar{\mu}\phi D_L} + \left(\frac{\pi^2}{L^2\gamma^2} + 1\right)\frac{V}{\phi D_L}\frac{d\psi}{dc}\right]\frac{\partial\bar{c}}{\partial z} = \left(\frac{\pi^2}{L^2\gamma^2} + 1\right)\left(\frac{\pi^2}{L^2\gamma^2} + 1\right)\gamma^2 . \tag{7.45}$$

Coskuner and Bentsen [1989] defined the wave number γ (when m=n=1) as

$$\gamma^2 = \left(\frac{\pi}{L_x}\right)^2 + \left(\frac{\pi}{L_y}\right)^2 . \tag{7.46}$$

Considering Equation (7.46) and the expression for N_c , one can rewrite Equation (7.45) as follows:

$$\left[\frac{k\left(\frac{V}{k}\frac{d\mu}{dc} - \frac{d\rho}{dc}g\right)\psi(\bar{c})}{\bar{\mu}\phi D_L} + \left(\frac{1}{\Omega} + 1\right)\frac{V}{\phi D_L}\frac{d\psi}{dc}\right]\frac{\partial\bar{c}}{\partial z} = \pi^2\left(\frac{1}{\Omega} + 1\right)\left(\frac{1}{\Omega} + K\right)\frac{L_x^2 + L_y^2}{L_x^2 L_y^2} , \tag{7.47}$$

where,

$$\Omega = \frac{L^2(L_x^2 + L_y^2)}{L_x^2 L_y^2} . \tag{7.48}$$

If the instability number I is defined as

$$I = \left[\frac{k\left(\frac{V}{k}\frac{d\mu}{dc} - \frac{d\rho}{dc}g\right)\psi(\bar{c})}{\bar{\mu}\phi D_L} + \left(\frac{1}{\Omega} + 1\right)\frac{V}{\phi D_L}\frac{d\psi}{dc}\right]\frac{\partial\bar{c}}{\partial z}\,\frac{\frac{L_x^2 L_y^2}{L_x^2 + L_y^2}}{\left(\frac{1}{\Omega} + 1\right)\left(\frac{1}{\Omega} + K\right)} , \tag{7.49}$$

then, the marginal instability condition is

$$I = \pi^2 . \tag{7.50}$$

7.4 Comparison with Coskuner and Bentsen's Theory

Coskuner and Bentsen [1989] have derived a dimensionless scaling group to predict the onset of an instability for miscible displacements where the standard diffusion equation was used, which has been tested by miscible displacements conducted in glass-bead packs. The instability number was defined as

$$I' = \left[\frac{k\left(\frac{V}{k}\frac{d\bar{\mu}}{d\bar{c}} - \frac{d\rho}{d\bar{c}}g\right)}{\bar{u}\phi D_L}\frac{\partial\bar{c}}{\partial z}\right]\frac{\dfrac{L_x^2 L_y^2}{L_x^2 + L_y^2}}{\left(\dfrac{1}{\Omega}+1\right)\left(\dfrac{1}{\Omega}+K\right)} . \tag{7.51}$$

Note that the difference between I and I' is caused by $\psi(\bar{c})$ and $d\psi(\bar{c})/dc$. For a homogeneous porous medium where H equals one, $\psi(\bar{c})$ and $d\psi(\bar{c})/dc$ are one and zero, respectively. In such a case, the two instability numbers, I and I', become identical. Although it is not clear how heterogeneity affects the onset and development of instability, it is reasonable to assume that the heterogeneity is favorable for the generation of instability. In this regard, the instability number, I, must be greater than the instability number, I', which was derived by Coskuner and Bentsen, when the heterogeneity factor H is greater than 1. This yields $\psi(\bar{c}) > 1$, provided that the increase in the magnitude of the instability number, I, due to the second term in the bracket on the right hand side of Equation (7.49) can be neglected; conservatively, that is,

$$\bar{c} < \frac{\sqrt{H} - 1}{H - 1} . \qquad (7.52)$$

Equation (7.52) indicates a possible unstable region within the transition zone. When H approaches infinity, $\bar{c}$ approaches zero. When H is one for homogeneous rock, $\bar{c}$ equals 0.5, which means that, if a porous medium is homogeneous, the possible unstable region is in the transition zone between the two points where $\bar{c}$ is 0 and 0.5. The more heterogeneous the porous medium is, the closer the unstable region is to the flood front where $\bar{c}$ is zero. Dumore [1964] proposed a stability criterion for downward miscible displacement, which indicates that the part of transition zone adjacent to the displaced fluid is in an unstable position when the displacement velocity is greater than the stable rate and less than the critical rate. Lee et al. [1984] also pointed out that the most unstable point is ahead of the point where c=0.5. The agreement of Equation (7.52) with Dumore and Lee's inference suggests that the newly proposed model is capable of being used together with linear perturbation theory.

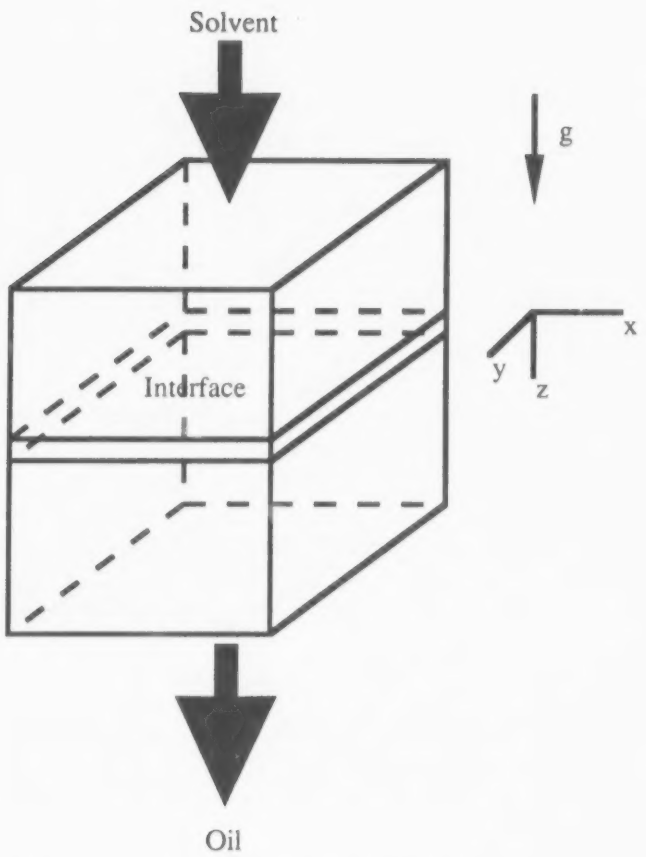

Figure 7.1 A Downward Miscible Displacement

8. EXPERIMENTAL

In order to test the mathematical model derived in Chapter 4, a series of miscible displacements were performed to measure effluent histories. Miscible fluids having different viscosity ratios were used to investigate the effect of viscosity difference on the displacement performance. All displacements were conducted in a vertical sand pack model. The fluid with higher density was produced or injected at the bottom of the model and the fluid with lower density was produced or injected at the top of the model. By doing this, the effects of gravity segregation could be minimized. The porous sand pack was prepared carefully to make it uniform. Different displacement velocities were supplied by a Ruska pump. As a consequence, only the effect of viscosity ratio and displacement velocity has been investigated experimentally.

8.1 Description of Experimental Apparatus

A schematic diagram of the experimental apparatus used in this investigation is shown in Figure 8.1. There are essentially four parts in the system: 1) a sand-pack model used as a porous medium; 2) two reservoirs containing the displaced and displacing fluids; 3) a Ruska pump which provides a constant rate supply of injected fluid; 4) a receiver to collect effluent at the bottom or the top of the model, and an Abby type refractometer for concentration measurement of the effluent.

The sand pack model was made of plexiglass and sealed by epoxy. The two ends were connected with inlet and outlet lines, respectively. The plexiglass holder was filled with 60 - 120 mesh silica sand. The dimension of the sand pack is 1000x7.5x10 mm. The porosity and absolute permeability of the sand pack are

30.7% and 1.58 darcy, respectively. A Ruska pump was used to provide constant injection rates over a range of 8.5 to 560 cc/hr.

8.2 Experimental Procedure

The silica sand which was used to pack the model was 60 to 120 mesh. First, the sand was pre-treated with HCL acid for four hours and then flushed by distilled water. The clean but wet sand was put into an oven at about 300°C to remove the residual water. The dry sand was poured into the vertically placed model through the open end at the top. During the process, the sand was compacted by tapping the model with a rubber hammer.

To measure the pore volume and the absolute permeability of the sand pack, the sand pack was placed under vacuum until the pressure was 0.001mmHg. Then, distilled water was allowed to imbibe into it. The amount of imbibed water was measured and considered to be the pore volume of the sand pack. After the measurement of the pore volume, water was injected into the sand pack continuously at a constant rate by the Ruska pump. At the same time, the pressure difference at the inlet and outlet end was measured with a manometer.The Ruska pump was set to another rate, and another pressure difference was measured. Darcy's law was used to calculate the absolute permeability. The average of three measurements was considered to be the absolute permeability value of the sand pack.

Before the beginning of a displacement, the porous medium must be saturated entirely with the displaced fluid. To this end, the displaced fluid was injected into the sand pack using the Ruska pump. For the first two pore volume's of injection, the injection rate may be set as high as 50 cc/hr. Then, the rate was

decreased to the magnitude which was the desired displacement velocity, for another one and half pore volume's injection, or until the produced fluid was the same as that which was injected. After the sand pack was saturated, the displacement started with the injection of the displacing fluid at a constant rate. The produced fluid was collected with a graduated receiver. The weight of the effluent was measured and then converted into volume by its density measured with a densitometer. The concentration of the displacing fluid in the effluent was also measured with an Abby refractometer. Before breakthrough of the displacing fluid, measurements were made for every 10 cc of effluent produced. After that, measurements were performed for each 2 - 5 cc of production. Each measured value was assumed to be representative of the fluid passing the end of the sand pack during the small time interval. For each run, the displacement was continued until approximately 1.5 to 2 pore volumes of displacing fluid were injected.

Water and a mixture of water and glycerine were used as the two miscible fluids. By changing the concentration of glycerine in the solution, different viscosities of the mixtures can be obtained. Figure 8.2 shows the viscosities of the glycerine solution at a temperature of 30^{o}C.

Water and glycerine have different refractive indices. Figure 8.3 shows the refractive index of the glycerine solution, at a temperature of 30^{o}C, measured with an Abby type refractometer. From this figure, it can be seen that the refractive index of the solution depends linearly on the volume per cent of glycerine in the glycerine-water mixture. To measure the concentration of the displacing fluid in the effluent, the refractive index of the effluent is determined and then converted into concentration according to Figure 8.3.

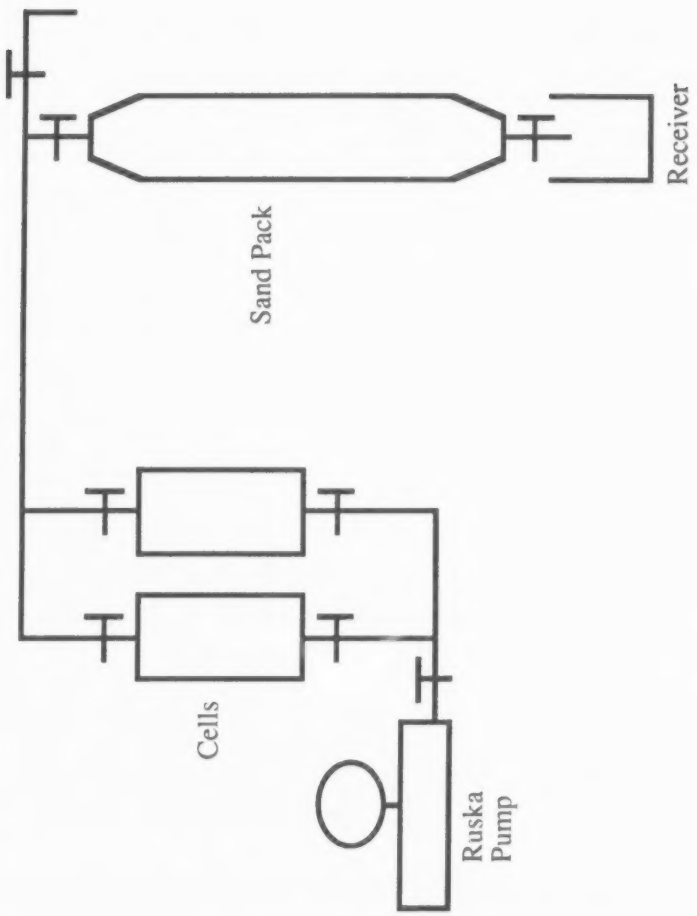

Figure 8.1 Schematic Drawing of
Experimental Apparatus

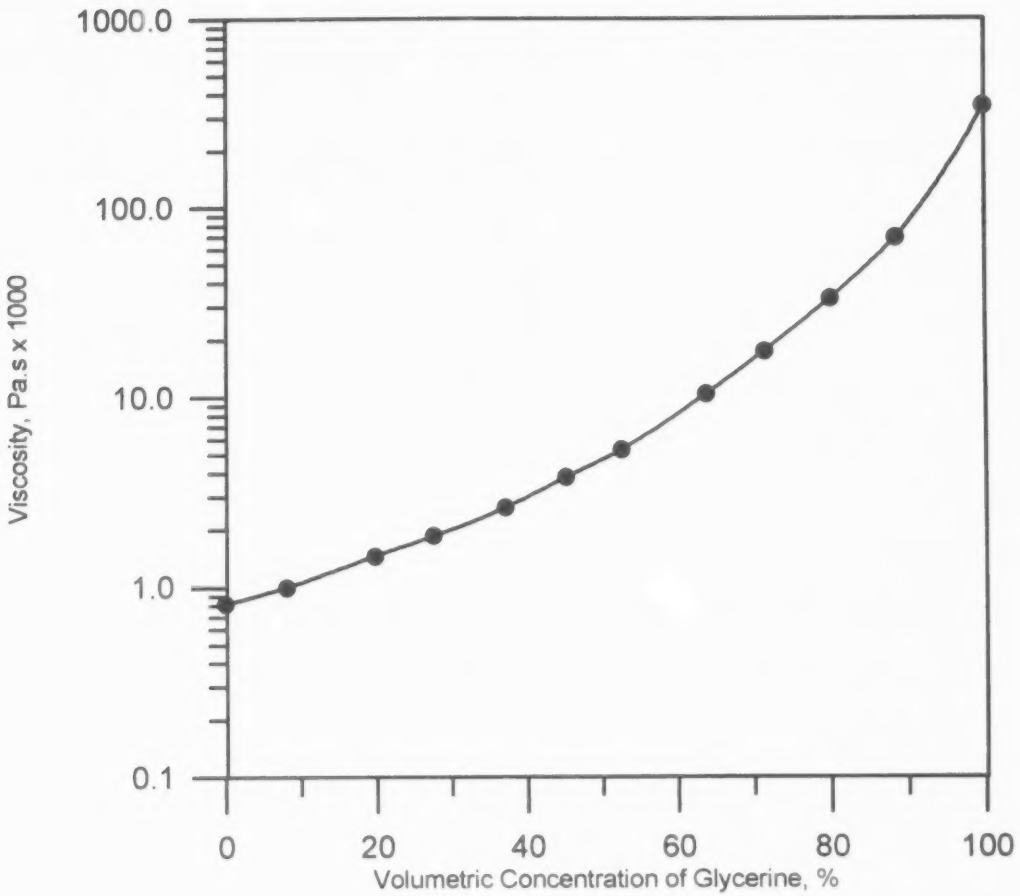

Figure 8.2 Viscosity of Glycerine Solution

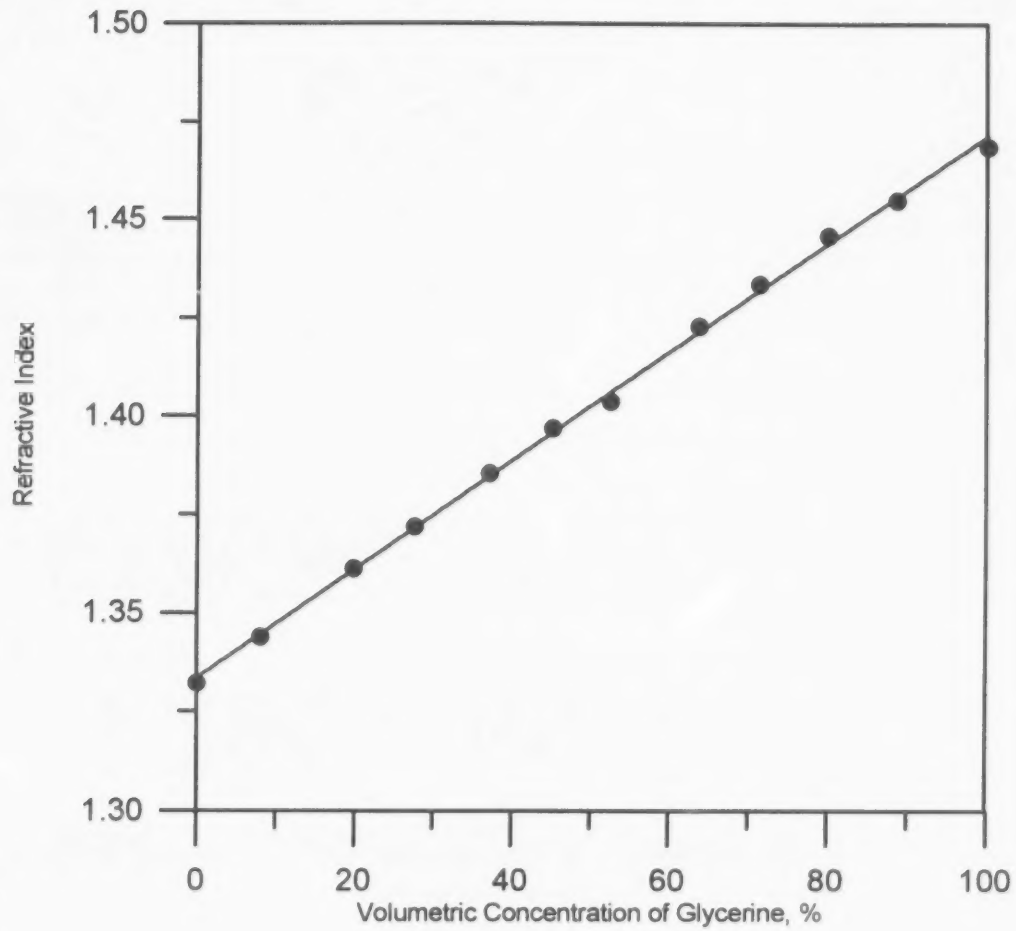

Figure 8.3 Refractive Index of Glycerine Solution

9. EXPERIMENTAL RESULTS AND DISCUSSION

The purposes of this experimental investigation were: 1) to perform miscible displacements using fluids with different viscosities; 2) to test the ability of the new model derived in Chapter 4 to predict the effluent history of a miscible displacement; 3) and to evaluate the effects of viscosity ratio and displacement velocity on the performance of a miscible displacement.

The results of a series of miscible displacements conducted in a homogeneous sand pack are presented in this chapter. Four different pairs of miscible fluids with different viscosity ratios were used in this laboratory investigation. The properties of the fluids used are listed in Table 9.1. The injection rates, which were obtained using a Ruska pump, ranged from 10 cc/hour (0.32 m/day) to 80 cc/hour (2.59 m/day).

Three groups of displacements were conducted using fluids with unfavorable viscosity ratios, while one group of displacements was performed using favorable-viscosity-ratio fluids. Similar experimental work has been done [Brigham et al., 1961]. But the displacement velocities were so high (greater than 5 m/day) that immiscible displacement theory can be used to approximate the process [Koval, 1963; Udey and Spanos, 1991; Udey and Spanos, 1993]. At low flow rates, the effects of longitudinal dispersion may not be neglected. Zhang [1993] pointed out that she noticed near "S"-shaped effluent curves even when unfavorable-viscosity-ratio fluids were used, provided that the displacements were stable. But no experimental data were given in her thesis.

9.1 Comparisons of Effluent Curves with Theoretical Predictions

All displacement tests were conducted at a constant flow rate. The displacing fluid, which was first-contact miscible with the displaced fluid at all proportions, was injected into the sand pack continuously. The dimensionless time was obtained by dividing the measured volume of the injected fluid by the pore volume of the sand pack. The mathematical model, Equation (4.30), together with initial and boundary conditions, Equations (4.31) through (4.33), was solved to give the fractional flow of the displacing fluid at the outlet end; that is the effluent curve or history. In the theoretical calculation, two parameters, P_e and HE, were adjusted to yield the best match with the corresponding experimentally determined effluent curve. Because the porous medium used in this study is a sand pack, which is believed to be homogeneous, the heterogeneity factor, H, for the sand pack is assumed to be one.

9.1.1 Displacements with Favorable Viscosity Ratios

Figure 9.1 shows the effluent curves of miscible displacements using fluids with a favorable viscosity ratio of 0.24 for three different flow rates. According to Coskuner and Bentsen [1989], miscible displacements using favorable-viscosity-ratio fluids are stable if the displacements are conducted in a homogeneous porous medium. As a consequence, the effluent curves for the three different rates all have a symmetric "S" shape, as shown in Figure 9.1. It can be seen from the figure that the effluent curves coincide quite well for the different flow rates. Furthermore, the dimensionless transition zone length, around the breakthrough time of the displacing fluid, can be obtained from the curves, and is estimated to be about 0.07.

The characteristics of a miscible displacement using fluids with a favorable viscosity ratio are a narrower effluent curve, which indicates a narrower transition

zone, and a symmetric "S"-shaped effluent curve. The narrower transition zone implies a more efficient displacement result. This may be caused by the reduction in dispersion and/or by the favorable viscosity ratio. The standard dispersion-convection equation may be used to match the effluent curves shown in Figure 9.1 because they have a symmetric "S" shape. The solution to the standard dispersion-convection equation was given by Brigham [1974] as follows:

$$f_s = \frac{1}{2}\,\mathrm{erfc}\left(\frac{1-\tau}{2\sqrt{\tau/P_e}}\right) + \frac{1}{2\sqrt{\pi P_e \tau}}\, e^{-\left(\frac{1-\tau}{2\sqrt{\tau/P_e}}\right)^2} \qquad (9.1)$$

If Equation (9.1) is used to match the effluent curves shown in Figure 9.1, only one parameter, the Peclet number, is adjustable. This means that the transition zone growth and the effluent history are controlled solely by dispersion. A narrower transition zone necessitates lower dispersion; hence, a higher Peclet number. Consequently, a Peclet number of about 4500 is required to match the effluent curves as shown in Figure 9.1. Because, when the Peclet number is higher than 3000, the change in the effluent curve is not very sensitive to P_e, the Peclet number of 4500, which is obtained through matching calculations, is an approximate result.

The new model, Equation (4.30), also predicts a symmetric "S"-shaped effluent curve when the product of H and E is equal to or less than one. To match the effluent curves shown in Figure 9.1 using the new model, a combination of Peclet number, 250, and effective viscosity ratio, 0.59, is found by comparing the predicted effluent curves with the experimentally determined ones. The agreement is reasonably good as shown in Figure 9.1. Other combinations are also possible if only the effluent curve is to be matched. Note, however, that the width of the transition zone depends on two factors: the Peclet number and the effective

viscosity ratio. If the narrowing of the transition region is attributed to a reduction in dispersion, and if the effective viscosity ratio is taken to be one, a Peclet number of about 4500 is needed to match the effluent curve. Under these circumstances, the new model and the traditional convective-dispersion model become identical. If the narrowing of the transition zone is brought about partly by a favorable viscosity ratio, a Peclet number of 250 is needed to match the effluent curve, if the effective viscosity ratio is set equal to 0.59.

Although different models and different values of the parameters can yield the same effluent history, the behavior of the transition zone growth depends markedly upon the approach used. The transition zone length predicted by Equation (2.1) in an one-dimensional system is given by Walsh and Withjack [1993]:

$$\lambda_{3.5\% - 96.5\%} = 5.12 \sqrt{\frac{\tau}{P_e}} \qquad (9.2)$$

Equation (9.2), together with the matched Peclet number of 4500, and the new model, Equation (4.30), together with the matched Peclet number of 250 and the matched effective viscosity ratio of 0.59, are used to calculate the transition zone growth with dimensionless time. The results are shown in Figure 9.2. Because no experimental data on the transition zone growth in this study are available, it is impossible to say which is correct. But it is very important to notice that, although the transition zone length around the breakthrough time predicted using the two approaches is almost the same, the growth of the transition zone at early time differs significantly. With the new model, Equation (4.30), the lower Peclet number of 250 indicates more pronounced dispersion. Therefore, the transition zone grows rapidly, during the early stages, when the concentration gradient is the greatest. As

the displacement goes on, the concentration gradient decreases and the effect of the favorable viscosity ratio becomes more pronounced, dampening the growth of the mixing zone. The new model, Equation (4.30), properly accounts for the effect of the interplay between dispersion and effective viscosity ratio on the behavior of transition zone growth. The traditional model, Equation (2.1), together with a high but unchanged value of Peclet number, predicts that the transition zone length growth is caused and controlled solely by dispersion. As can be seen from Figure 9.2, the transition zone length calculated using Equation (9.2) does not grow as rapidly as that calculated using the new model; rather, it grows steadily with the square root of time. Walsh and Withjack [1993] also noticed that the effluent curve of a miscible displacement conducted in a Berea sandstone could be matched using different models. But the different models predicted different rates of transition zone growth. Hence, it is very important to obtain information on mixing zone growth, in addition to the effluent history, for a better understanding of a miscible displacement taking place in a porous medium.

9.1.2 Displacements with Unfavorable Viscosity Ratios

When the fluids used have an unfavorable viscosity ratio, viscous "fingering" may occur. Thus, the displacement is not stable [Coskuner and Bentsen, 1989]. Figures 9.3 and 9.4 show the effluent curves obtained from the experimental data and the theoretical match calculations for two miscible displacements using fluids with viscosity ratios of 4.15 and 36.59, respectively [The rest of the curves are in Appendix A]. The flow rate for the two displacements is 0.00113 cm/s. As can be seen from the graphs, the breakthrough time of the displacing fluid becomes shorter for the displacements with a higher viscosity ratio.

Figure 9.3 shows a more rapid increase of the displacing fluid concentration, which implies a shorter transition zone length around the breakthrough time. It is also noticeable that disturbances exist among the experimental data, which indicates viscous "fingering" developed during the displacements.

Figures 9.3 and 9.4 show that the effluent curves are no longer symmetric "S"-shaped. The phenomenon of the distorted "long-tailing" effluent curve is more pronounced in Figure 9.4. In such a case, the traditional dispersion-convection equation with an error function type solution does not apply [Brigham, 1974]. The new model, Equation(4.30), is employed to match the elongated effluent curves by adjusting the Peclet number and the effective viscosity ratio. For Figure 9.3, where the viscosity ratio is 4.15, the matched parameters are: Pe =375; E=1.25. For Figure 9.4, where the viscosity ratio is 36.59, the matched Peclet number is 600 and the matched viscosity ratio is 1.75. Notice that the effective viscosity ratio is always less than its corresponding component viscosity ratio because dispersion can moderate the viscosity contrast when two miscible fluids contact. Nevertheless, the more mobile displacing fluid still tends to override the mixing front, resulting in an early breakthrough of the displacing fluid.

9.2 Breakthrough Recovery

Fluids with an adverse viscosity ratio give rise to early breakthrough of the displacing fluid. Recovery of the displaced fluid at the breakthrough time is called breakthrough recovery. The dimensionless time used in this study is defined as the volume of injected fluid divided by the total pore volume of the porous medium. Moreover, the amount of injected fluid is equal to the amount of produced fluid, prior to breakthrough of the injected fluid. As a consequence, the magnitude of the

breakthrough recovery is the same as that of the breakthrough time. It has been found that the effluent curve shifts to the left when a higher viscosity ratio is involved. Consequently, the breakthrough recovery becomes lower, which is caused by the override of the viscous "finger".

In this section, the breakthrough recovery data are compared with those calculated using the approximate analytical scheme. The Peclet number and the effective viscosity ratio are obtained through effluent-history-match calculations. Then, these two parameters are used in the breakthrough recovery calculation. The integral, I_O, defined by Equation (5.17), is a function of E, while the concentration, c, is a function of η, which is defined by Equation (5.8). Because it was assumed in Chapter 5 that the concentration c=0.5 travels at a constant velocity of u/ϕ and the concentration profile, $c(\eta)$, moves at the same speed, one has the following equation when the flood front just arrives at the outlet end of a one-dimensional porous medium:

$$\tau_b + \lambda = 1. \tag{9.3}$$

From Equations (9.3) and (5.26), an equation for τ_b can be derived as

$$\tau_b = \frac{1 - \tau_b}{a} - \frac{b}{a^2} \ln\left(\frac{a\,(1 - \tau_b) + b}{b}\right), \tag{9.4}$$

from which the breakthrough time (breakthrough recovery) can be solved for iteratively. If the dispersion is neglected, then the Peclet number approaches infinity. Based on this assumption, the breakthrough time has the following form:

$$\tau_b = \frac{1}{1+(15/4)\, I_o} \,. \tag{9.5}$$

Obviously, the breakthrough time is equal to one when the integral, I_o, approaches zero. This means that the displacement is a piston-like displacement when matched fluids are used and dispersion does not exist. If matched fluids are to be used and the dispersion is considered to control the process, a formula for the breakthrough time may be derived as

$$\tau_b = 1 + \frac{5}{P_e} - \sqrt{(1+\frac{5}{P_e})^2 - 1} \,. \tag{9.6}$$

It is clear that increased dispersion results in an earlier breakthrough. The breakthrough time approaches one when the Peclet number approaches infinity, which is the same conclusion as that drawn from Equation (9.5).

Table 9.2 shows the comparisons of the measured breakthrough recoveries with those calculated using Equation 9.4. From the table, it can be seen that a higher effective viscosity ratio and/or lower Peclet number give(s) rise to a reduced breakthrough recovery. Due to the disturbances existing among the experimental data, which are caused by instability of the displacement, it is difficult to determine the breakthrough time accurately. Hence, the comparisons here are not rigorous. Nevertheless, it is possible to point out that the calculated breakthrough recoveries are slightly higher than those measured for the displacements performed in this study. For Brigham's data, the predicted value of breakthrough recovery (52%), which is calculated using Equation (9.4) together with the parameters from the effluent-curve-match, is about 8% higher than the measured value. One possible reason for this difference may be that the velocities of the displacements conducted

in this study are much lower than those used in Brigham's displacements. In a lower flow rate displacement, more time is available for the molecules of the fluids to mix, which results in more complete mixing and a more pronounced dispersion effect. In this case, a longer "toe" on the concentration profile is expected. As a consequence, the approximate analytical scheme predicts a later breakthrough of the displacing fluid. It is also noticeable that the breakthrough recovery estimated from Brigham's data may not be accurate because there is not enough data around the breakthrough time, as shown in Figure 6.1.

9.3 Effective Viscosity Ratio

The effective viscosity ratio, defined in this study, is a complicated concept. It reflects the actual viscosity contrast of the fluids. But it is not equal to the value of the actual viscosity ratio because it is affected by other factors. In the derivation of the new model, Equation (4.19), the defining equation for F_S, includes a mobility ratio of the displacing solvent to that of the displaced oil. To make the problem tractable, the permeability ratio and viscosity ratio, which are affected by concentration, are considered separately.The permeability ratio may be assumed to be proportional to the ratio of the concentrations of the fluids [Jankovic, 1986]. Due to the mixing between the fluids, the effective viscosity ratio is usually taken to be some value less than that which pertains to the pure component viscosity ratio. Koval [1963] proposed a formula, Equation (4.22), for the effective viscosity ratio. His formula was based on a series of high flow rate miscible displacements, where dispersion can be neglected. In fact, macroscopic dispersion is influenced by displacement velocity [Perkins and Johnston, 1964]. As a consequence, the effective viscosity ratio, which is less than the normal viscosity ratio due to the

moderation of the viscosity contrast caused by dispersion, is influenced by displacement velocity. In this study, no attempt is made to propose a formula to calculate the effective viscosity ratio; rather, it is obtained by matching the predicted effluent history (Equation (4.30)) with the experimentally measured effluent curve.

Figure 9.5 presents the effective viscosity ratios. It may be seen from the graph that the effective viscosity ratio increases almost linearly with the displacement velocity. The three curves also demonstrate a trend that the effective viscosity ratio approaches approximately one when the displacement velocity approaches zero. When the displacement velocity decreases, the transverse dispersion may have more time to suppress the initiation and development of viscous fingers. Another possible reason may be that dispersion has more influence on the displacement performance at a lower flow rate. Hence, it may be inferred that, at very high flow rates, the effective viscosity ratio may approach a fixed value because dispersion has little effect on the process at high velocities.

It can also be seen from Figure 9.5 that, as the viscosity ratio increases, the effect of displacement velocity on the effective viscosity ratio increases. For example, when the viscosity ratio is 4.15, the effective viscosity ratio increases only from 1.25 at 0.0011 cm/s to 1.46 at 0.037 cm/s. But for the viscosity ratios of 8.54 and 36.59, the effective viscosity ratios increase more rapidly with displacement velocity .

9.4 Dispersion Coefficient

Liquid dispersion in a porous medium is affected not only by the properties of the fluids, but also by the properties of the porous medium and by the flow rate. The effective macroscopic dispersion coefficient, which was proposed to account

for the total effect of dispersion, was assumed to be the sum of the molecular diffusion and the convective dispersion coefficient [Perkins and Johnston, 1964]. The molecular diffusion in a porous medium is mainly controlled by the properties of the fluids and the porous medium. Hence, it is not affected by flow rate. The convective dispersion coefficient was found to be dependent on velocity [Perkins and Johnston, 1964].

If the effluent history of a miscible displacement can be modeled by the traditional dispersion-convection equation, the effective dispersion coefficient can be determined using the straight line method [Brigham et al., 1961]. In this study, the new model, Equation (4.30), is used to match the effluent curves. Because of the disturbances among the experimental data, the matched Peclet numbers are not accurate. So the dispersion coefficient calculated from the matched Peclet number is not accurate either. But still, some trends may be seen from the data.

Figure 9.6 shows the dispersion coefficients changing with viscosity ratio for the displacements with velocities of 0.00113 cm/s and 0.00038 cm/s, respectively. The dispersion coefficient decreases as the viscosity ratio increases. Brigham et al.[1961] performed a group of miscible displacements using favorable viscosity ratios of 0.175 and 0.998. When the viscosity ratio increased from 0.175 to 0.998, they found that the mixing rate decreased accordingly. As discussed in Section 9.1.1, one of the reasons for the reduced mixing rate may be a favorable viscosity ratio. But when Fick's law is used to describe the dispersion in a liquid phase, the dispersion coefficient changes significantly with concentration [Lydersen, 1983]

Figure 9.7 shows how displacement velocity affects the dispersion coefficient. For all three viscosity ratios of 4.15, 8.54 and 36.59, it is observed that the dispersion coefficient increases with increasing displacement velocity. The three

curves seem to converge at low flow velocities. This is expected because, at low flow velocities, molecular diffusion dominates the longitudinal mixing and the dispersion coefficient is independent of flow velocity. At high flow velocities, convective dispersion dominates the longitudinal mixing and the dispersion coefficient becomes dependent on flow velocity. Brigham et al. [1961] suggested that the dispersion coefficient increases with flow rate according to

$$D_L = \alpha\, u^{1.2} . \tag{9.7}$$

From Figure 9.7, it is observed that the data are not sufficient to draw a relationship, but it is clear that the dispersion coefficient increases with increasing velocity. Especially when the flow velocity is greater than 0.0015 cm/s, the dispersion coefficient increases with increasing flow rate almost linearly.

9.5 Effects of Flow Rate and Viscosity Ratio on the Effluent Curve

An effluent curve reflects the transition zone passing through the outlet end of a porous medium. The breakthrough time, the time period for the transition zone to pass the outlet end and the shape of the effluent curve indicate how the mixing takes place in a displacement.

If a viscosity ratio is favorable, the effect of flow velocity is not detectable when the velocity is greater than 0.00113 cm/s, as shown in Figure 9.1. If the standard dispersion-convection equation is used to describe the dispersion behavior, the Peclet number obtained from the match calculation should be the same for the three cases. According to the definition for the Peclet number, Equation (4.29), the dispersion coefficient must be proportional to the flow velocity to keep

the Peclet number unchanged when the velocity increases. If the new model, Equation (4.30), is used to describe the displacement behavior, two parameters, the effective viscosity ratio and the Peclet number, can be adjusted. In this case, it is questionable to say that the Peclet number is the same for the three velocities. Hence, it is impossible to draw a conclusion that the dispersion coefficient is proportional to the flow velocity. As discussed in Section 9.1.1, additional information is needed for the purpose of choosing a proper model [Walsh and Withjack, 1993].

Shown in Figure 9.8 are the effluent curves for three displacement velocities: 0.00038 cm/s, 0.00075 cm/s and 0.00113 cm/s. The viscosity ratio for the three displacements is 8.54. It can be seen from the graph that increasing the flow velocity results in an early breakthrough of the displacing fluid. The time period for the transition zone to pass the outlet end also becomes longer, which means that more displaced fluid is left behind the flood front after breakthrough. To achieve the same recovery, more displacing fluid must be injected. It is also noticeable that the disturbances become more pronounced as the velocity increases. Both the amount of dispersion and effective viscosity ratio increase as the flow velocity increases. An increased dispersion coefficient and an increased effective viscosity ratio both result in a reduction in displacement efficiency or recovery of the displaced fluid. So it is desirable to reduce the displacement velocity in a practical miscible flooding project to achieve a high oil recovery. At low flow velocities, the transverse dispersion may alleviate the recovery reduction caused by viscous fingering, although it can not prevent completely the formation and development of viscous fingers [Blackwell et al., 1959].

An unfavorable viscosity ratio is always an adverse factor for oil recovery, either for immiscible or miscible displacement. Figure 9.9 presents the effluent

curves for three viscosity ratios: 4.15, 8.54 and 36.59. The displacement velocity for the three cases is 0.00113 cm/s. It is very clear that increased viscosity ratio gives rise to a decreased breakthrough recovery. For example, when the viscosity ratio is 4.15, the breakthrough recovery is about 67%. When the viscosity ratio is increased to 36.59, the breakthrough recovery is decreased to 51%. A larger volume of displacing fluid is needed for the concentration of displacing fluid to reach one. From the graph, if the viscosity ratio is 4.15, about 1.5 pore volumes of displacing fluid can displace the displaced fluid completely. If the viscosity ratio is 36.59, about 2.0 pore volumes of displacing fluid must be injected for a complete displacement of the displaced fluid. If the porous medium is heterogeneous, a reduction in the volumetric sweep efficiency caused by the adverse viscosity ratio would be expected in addition to the reduction in the unit displacement efficiency. The displacing fluid used in a miscible flooding project is usually less viscous than the reservoir oil. An adverse viscosity ratio is difficult to avoid. Therefore, it is very important to use other techniques to stabilize the miscible flooding front for a high sweep efficiency.

9.6 Discussion of Errors

Because most of the displacements conducted in this study were unstable, the concentrations of displacing fluid in effluent after breakthrough fluctuate significantly. The method of determining the concentration of effluent at a given time is to measure the refractive index of a certain amount of the effluent produced during a certain amount of time. The effluent curve measured using this method would be smoother than that measured with an ideal instant concentration instrument.

Another error may be introduced by the density difference of the fluids. The maximum difference in density is 0.197 according to Table 9.1. In all displacements, flow is vertical and the heavier fluid is always injected at the bottom of the porous medium or the lighter fluid is injected at the top of the porous medium. This favorable density difference may help to suppress the formation and growth of viscous fingers [Blackwell et al., 1959]. If this is true, the measured effluent curve may be smoother and may show a more optimistic result than is expected when using fluids with equal density.

The errors in pore volume and permeability measurements have no significant effect on the shape of the effluent curve or on the calculations, provided that they do not change significantly during the displacement test. This assumption is generally acceptable.

Table 9.1 Properties of the Miscible Fluids

displacing fluid				
	1	2	3	4
viscosity(Pa.s)	$3.41*10^{-3}$	$0.82*10^{-3}$	$0.82*10^{-3}$	$0.82*10^{-3}$
density(g/cm^3)	1.1038	0.9952	0.9952	0.9952
refractive index	1.4004	1.3322	1.3322	1.3322
displaced fluid				
viscosity(Pa.s)	$0.82*10^{-3}$	$3.41*10^{-3}$	$7.0*10^{-3}$	$30.0*10^{-3}$
density(g/cm^3)	0.9952	1.1038	1.1417	1.1922
refractive index	1.3322	1.4004	1.4143	1.4432

Table 9.2 Breakthrough Recovery : Experimental and Matched

μ_o/μ_s	10^3*u cm/s	E	I_o	P_e	R_b	R_{bc}	10^3*D_L cm^2/s
4.15	1.13	1.25	0.076	375	0.67	0.68	0.031
4.15	1.88	1.39	0.110	250	0.62	0.63	0.075
4.15	3.00	1.47	0.130	250	0.58	0.61	1.201
8.54	0.38	1.11	0.036	300	0.76	0.75	0.125
8.54	0.75	1.25	0.076	350	0.70	0.70	0.215
8.54	1.13	1.43	0.120	400	0.61	0.64	0.282
36.59	0.38	1.33	0.090	400	0.68	0.70	0.094
36.59	1.13	1.75	0.180	600	0.51	0.57	0.188
5.71 Brigham	6.00	1.33	0.09	50	0.60	0.52	

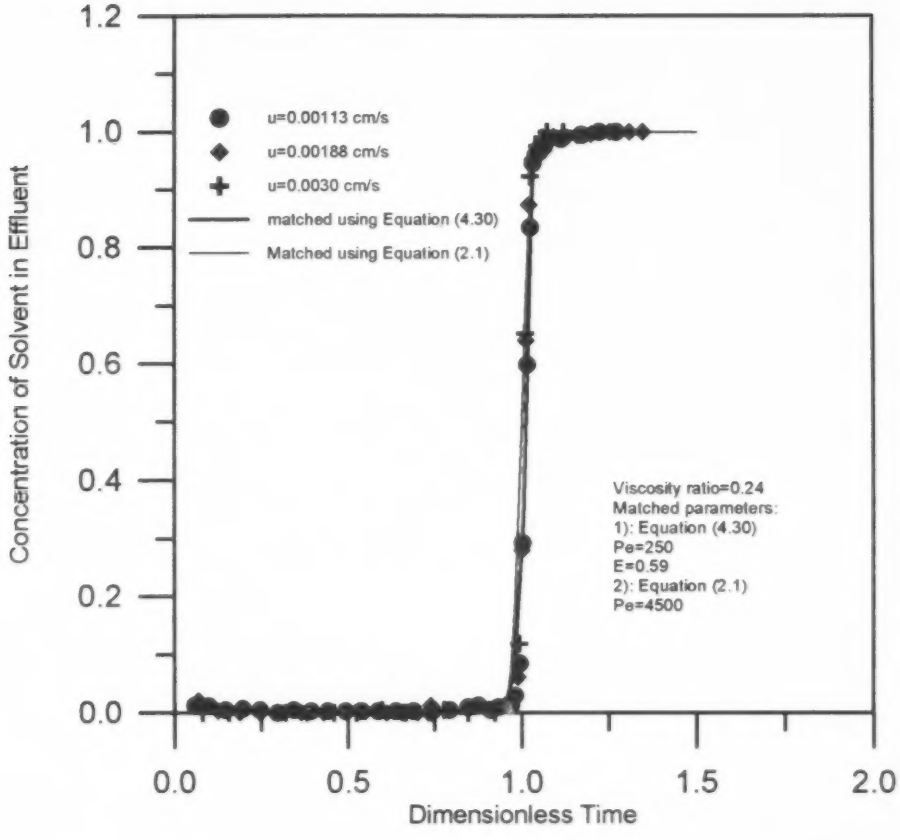

Figure 9.1 Effluent Curves of Displacements Using Fluids with Favorable Viscosity Ratios

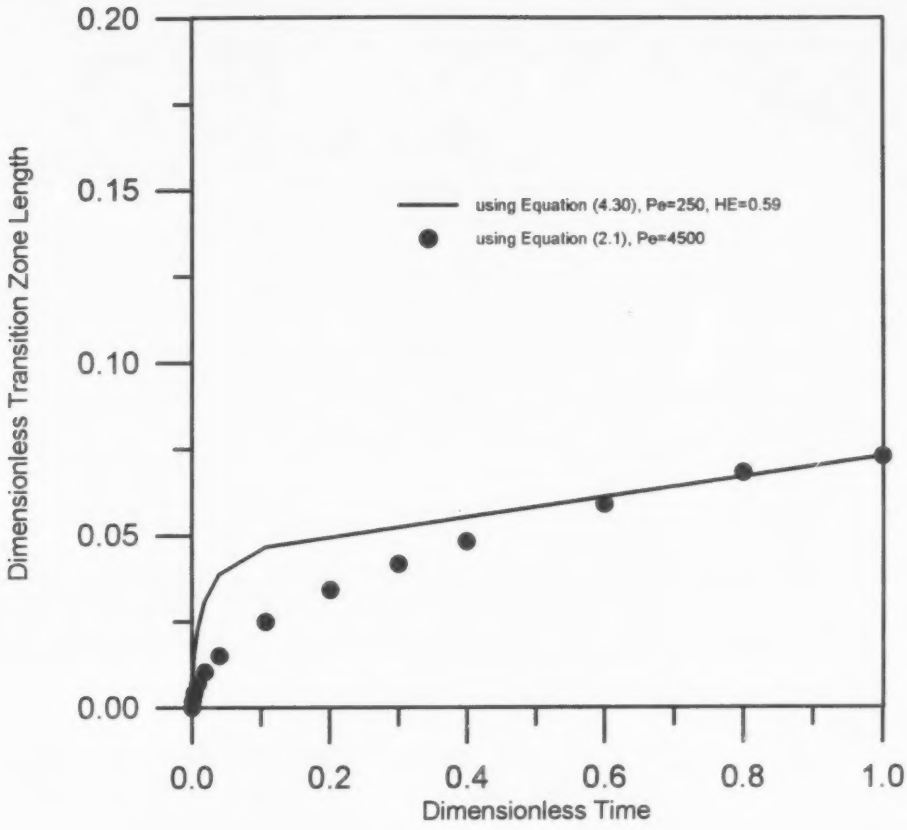

Figure 9.2 Transition Zone Growth Using Different Models

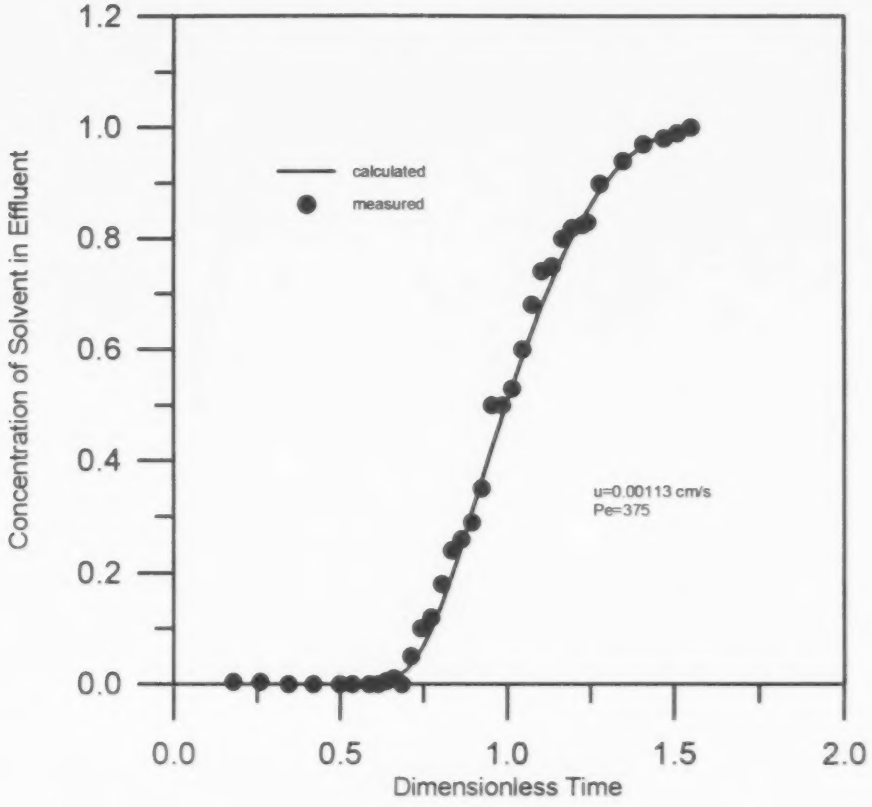

Figure 9.3 Effluent Curves: Experimental versus Predicted
Viscosity Ratio = 4.15

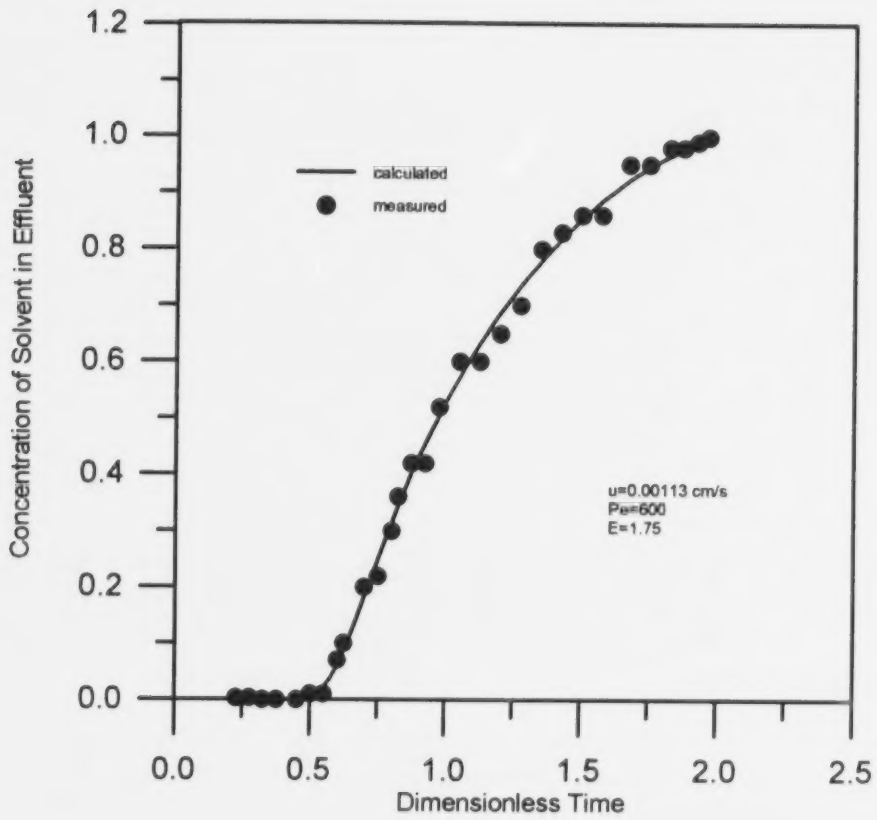

Figure 9.4 Effluent Curves: Experimental versus Predicted
Viscosity Ratio = 36.59

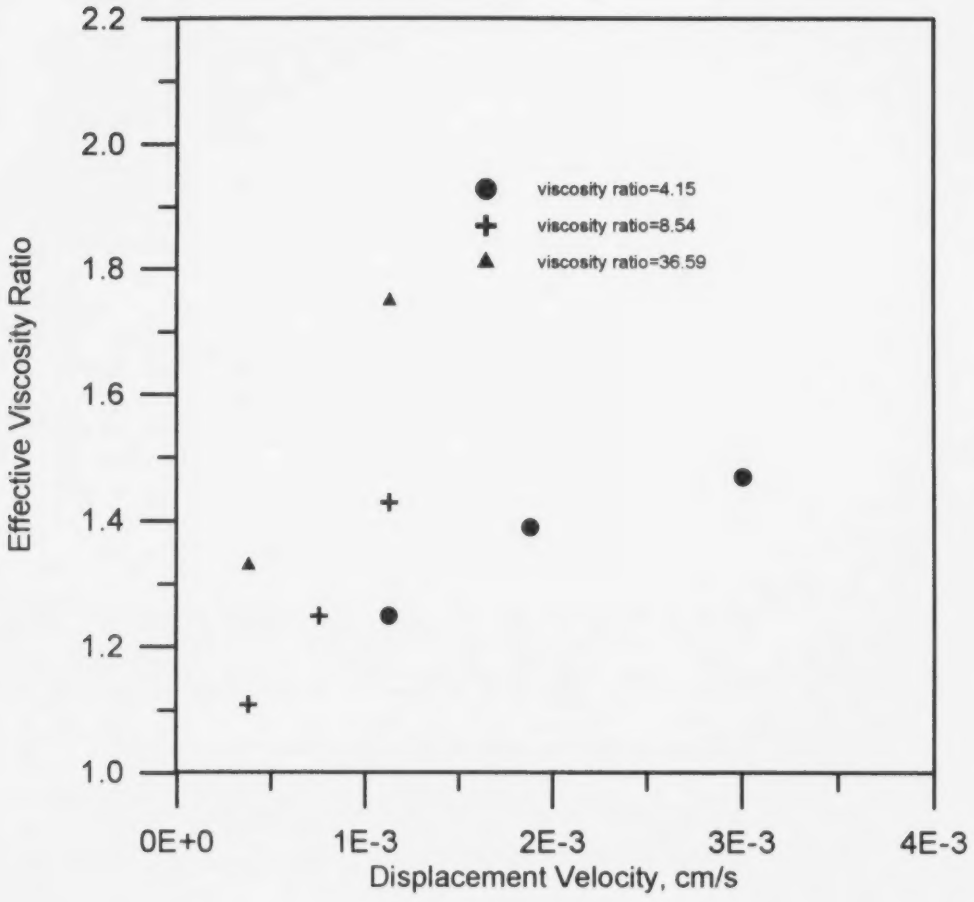

Figure 9.5 Effective Viscosity Ratio Changes with Velocity

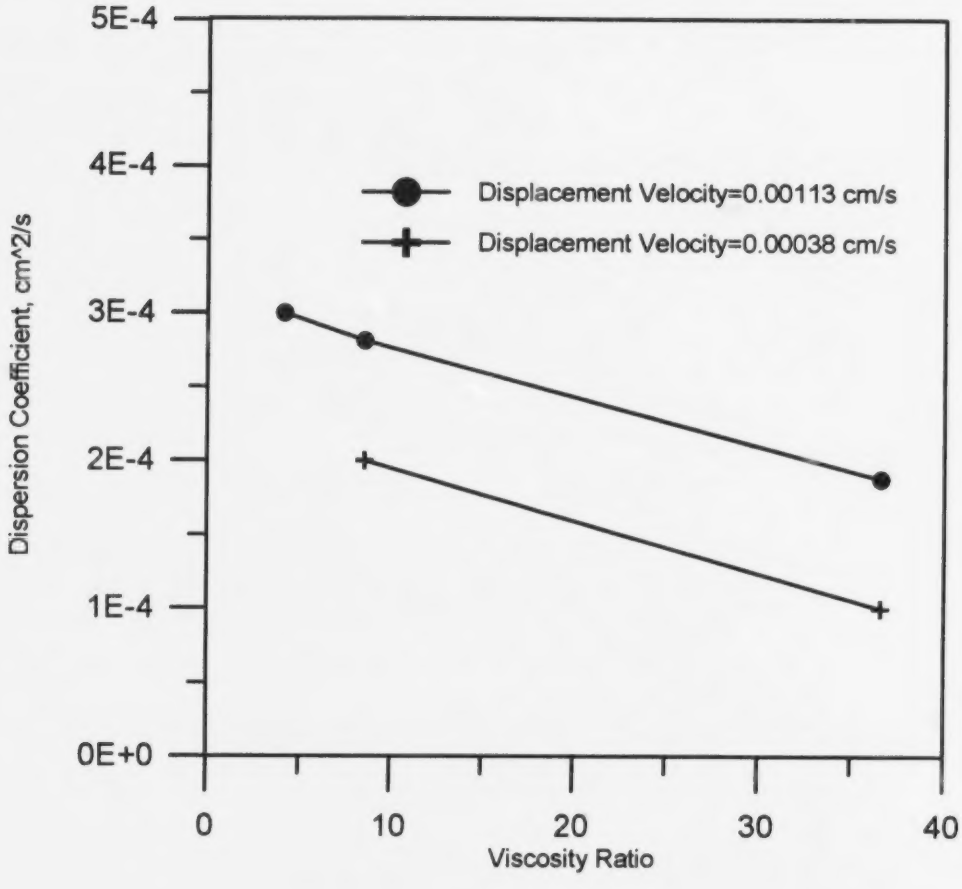

Figure 9.6 Dispersion Coefficient Changes with Viscosity Ratio

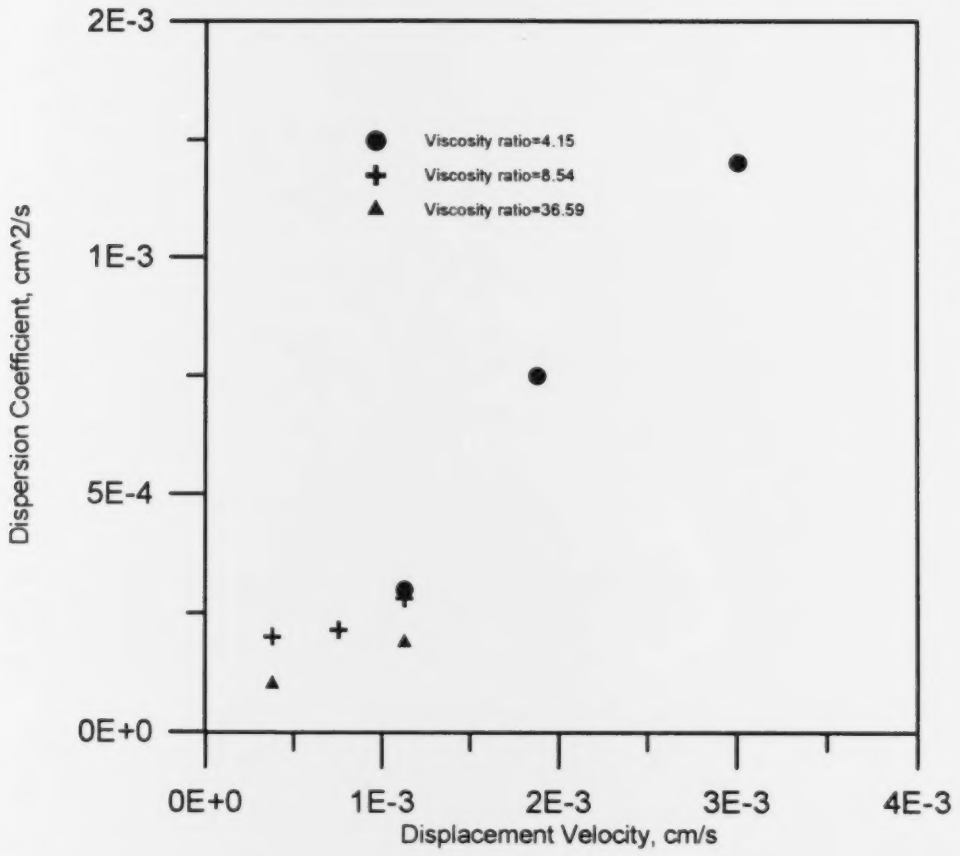

Figure 9.7 Dispersion Coefficient Changes with Velocity

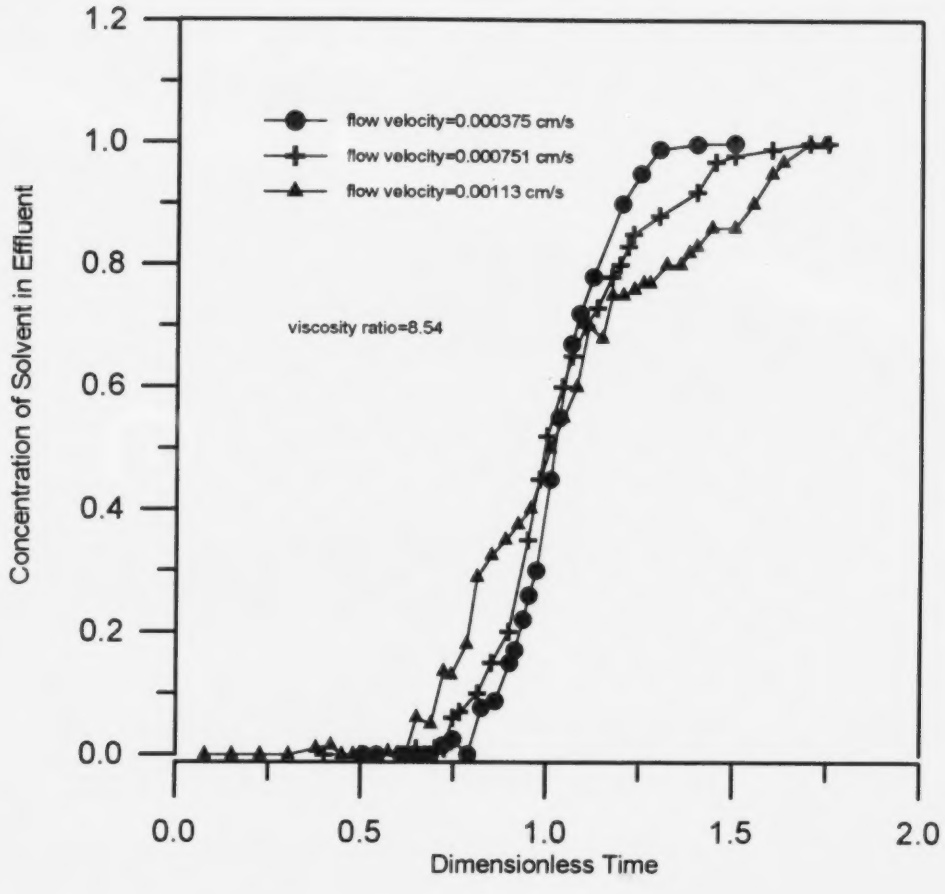

Figure 9.8 Effluent Curves for Different Displacement Velocities

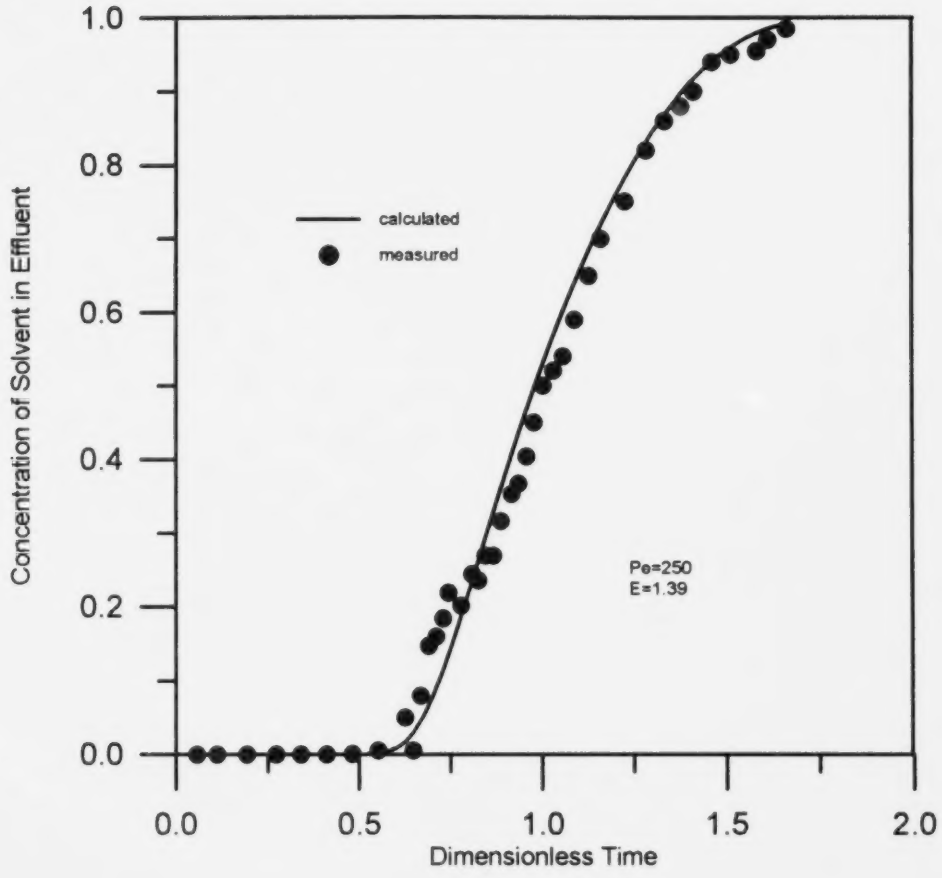

Figure A.1 Effluent Curves: Experimental versus Matched Viscosity Ratio=4.15, Velocity=0.00188 cm/s

10. SUMMARY AND CONCLUSIONS

A new mathematical model for one-dimensional miscible displacement has been proposed, which includes the viscosity ratio and the heterogeneity factor explicitly. An approximate analytical solution to the new model has also been found. Furthermore, a linear perturbation theory was employed, together with the new model, to obtain perturbation equations which were solved using a variational technique. Then, a dimensionless scaling group and its critical value at the onset of instability for miscible displacements in heterogeneous porous media was derived.

A vertical sand pack was used to carry out a series of miscible displacements in which the viscosity ratio and flow rate were changed. The effluent curves measured from the displacements were matched using the new model. Keeping in mind the limitations of the new model, and for the experiments performed herein, the following conclusions may be drawn:

1. The new model was used successfully to match effluent curves and transition zone length data published in the literature and the effluent histories of the miscible displacements conducted in this study.

2. An approximate analytical solution to the new model was found and it demonstrated that the transition zone of a miscible displacement grows with the square root of time at early stages when the concentration gradient is the greatest. As the displacement goes on, the transition zone growth increases linearly with time when dispersion becomes negligible.

3. Theoretical analysis based on linear perturbation theory, together with the new model, indicates that the miscible displacements conducted in a heterogeneous porous medium have larger instability numbers than those conducted in a homogeneous medium, if other conditions are kept unchanged.

4. The effective viscosity ratio used in this study appears to become larger with increasing flow velocity.

5. Higher dispersion coefficients and higher viscosity ratios reduce the displacement efficiency.

6. The dispersion coefficient decreases as the viscosity difference becomes larger and increases as the flow velocity becomes higher.

11. SUGGESTIONS for FUTURE STUDY

The following studies are suggested to extend the present study:

1. More miscible displacements using different viscosity ratios at different flow velocities should be performed to quantify the relationship between effective viscosity ratio and flow rate.

2. The heterogeneity factor should be correlated to a permeability variation coefficient or some other measurable parameter.

3. Miscible displacements should be conducted in heterogeneous porous media to test the scaling group for the prediction of the onset of instability.

4. Different functional forms for tilting the concentration profile should be tried to account for the deformation of the true concentration profiles caused by heterogeneity and viscosity ratio.

5. More effort should be made to include the gravity difference in the mathematical model and to extend it to other dimensions.

6 Miscible displacements should be conducted in porous medium models with different lengths to see if the dispersion coefficient, which is included in the new mathematical model, is scale dependent.

References

Aris, R and Amundson, N.R.: 1957, Some remarks on longitudinal mixing or diffusion in fixed beds, *AIChE J.* **3**, p. 280.

Auriault, J.L. and Lewandowska, J.: 1994, On the cross-effects of coupled macroscopic transport equations in porous media, *Transport in Porous Media* **16**, p. 31.

Baker, L.E.: 1977, Effects of dispersion and dead-end pore volume in miscible flooding, *SPE J.* **6**, p. 219.

Blackwell, R.J., Rayne, J.R. and Terry, W.M.: 1959, Factors influencing the efficiency of miscible displacement, *Trans. AIME* **216**, p.1.

Bretz, R.E. and Orr, F. M., Jr.: 1987, Interpretation of miscible displacements in laboratory cores, *SPERE* **11**, p. 492.

Brigham, W.E.: 1974, Mixing equations in short laboratory cores; *SPE J.* **2**, p. 91.

Brigham, W. E., Reed, P. W. and Dew, J. N.: 1961, Experiments on mixing during miscible displacement in porous media; *SPE J.* **3**, p. 1.

Chandrasekhar, S: 1961, *Hydrodynamic and Hydromagnetic Stability*, Clarendon Press, Oxford.

Coats, K.H. and Smith, B.D.: 1964, Dead-end pore volume and dispersion in porous media, *SPE J.* **3**, p. 73.

Coskuner, G.: 1987, Instability of miscible displacement, PhD thesis, University of Alberta.

Coskuner, G. and Bentsen, R.G.: 1989, Effect of length on unstable miscible displacement, *J. Canad. Petrol. Technol.* **28**(4), p. 34.

Deans, H.A.: 1963, A mathematical model for dispersion in the direction of flow in porous media, *SPE J.* **3**, p. 49.

Dougherty, E.L.: 1963, Mathematical model of an unstable miscible displacement, *SPE J.* **6**, p. 155.

Dumore, J.M.: 1964, Stability considerations in downward miscible displacements, *Trans. AIME*, **231**, p. 356

Fayers, F.J.: 1984, An approximate model with physically interpretable parameters for representing miscible viscous fingering, SPE paper No 13166 presented at the 59th Annual Technical Conference and Exhibition, Houston, Texas.

Hewett, T.A. and Behrens, R.A.: 1993, Considerations affecting the scaling of displacements in heterogeneous permeability distributions, *SPEFE* **12**, p. 258.

Hicks, P.J., Jr., Narayanan, K.P. and Dearn, H.A.: 1984, An experimental study of miscible displacements in heterogeneous carbonate cores using X-ray CT, *SPEFE* **3**, p. 55.

Houseworth, J.E.: 1993, Characterizing permeability heterogeneity in core samples from standard miscible displacement experiments, *SPEFE* **6**, p. 112.

Hove, A.O., Ringen, J.K. and Read, P.A.: 1987, Visualization of laboratory corefloods with aid of computerized tomography of X-rays, *SPERE* **5**, p. 148.

Jankovic, M.S.: 1986, Analytical miscible relative permeability curves and their usage with compositional and pseudo-miscible simulators, *Journal of Canadian Petroleum Technology*, **25**, p. 55

Koval, E.J.: 1963, A method for predicting the performance of unstable miscible displacement in heterogeneous media, *SPE J.* **6**, p. 145.

Kwok, W., Hayes, R.E. and Nasr-El-Din, H.A.:1995, Dispersion in consolidated sandstone with radial flow, *Transport in Porous Media*, **00**, p. 1

Lacey, J.W. Draper, A.L. and Binder, G.G., Jr.: 1958, Miscible fluid displacement in porous media, *Trans. AIME* **213**, p. 76.

Lee, S.-T., Gary, K.-M. and Culham, W.E.:1984, Stability analysis of miscible displacement processes, SPE paper No. 12631 presented at the SPE/DOE Fourth Symposium on Enhanced Oil Recovery held in Tulsa, OK.

Lydersen, L. A.: 1983, *Mass Transfer in Engineering Practice* , John Wiley & Sons, Chichester, p.16.

Neuman, S.P.: 1977, Theoretical derivation of Darcy's law, *Acta Mechanica* **25**, p. 153.

Nguyen, H.H. and Bagster, D.F.: 1979, Unstable miscible liquid-liquid displacement in porous media: a new model for predicting displacement performance in homogeneous beds", *The Chemical Engineering Journal* **18**, p. 103.

Oguztoreli, M. and Farouq Ali, S.M.: 1984, Mathematical treatment of the miscible displacement from porous media, *AIChE J.* **2**(1), p. 55.

Perkins, T.K. and Johnston, O.C.: 1964, A review of diffusion and dispersion in porous media, *Trans. AIME* **231**, p. 356.

Perrine, R.L.: 1963, A unified theory for stable and unstable miscible displacement, *SPE J* . **9**, p. 205.

Pickens, J.F. and Grisak, G.E.: 1981, Scale-dependent dispersion in a stratified granular aquifer, *Water Resource Res* . **17**, p. 1191.

Stalkup, F.I., Jr.: 1984, *Miscible Displacement*, Henry L Doherty Series, SPE, Monograph Volume 8.

Udey, N. and Spanos, T.J.T.: 1991, A new approach to predicting miscible flood performance, Paper No. 91-5 presented at the CIM/AOSTRA Technical Conference in Banff, Alberta.

Udey, N. and Spanos, T.J.T.: 1993, The equations of miscible flow with negligible molecular diffusion, *Transport in Porous Media* **10**, p. 1.

Vinegar, H.J.: 1986, X-ray CT and NMR imaging of rocks, *J. of Petrol. Technol.* **3**, p. 257.

Von Rosenberg, D.U.: 1956, Mechanics of steady state single-phase fluid displacement from porous media, *AIChE J.* **2**(1), p. 55.

Vossoughi, S., Smith, J.E., Green, D.W. and Willhite, G.P.: 1984, A new method to simulate the effects of viscous fingering on miscible displacement processes in porous media, *SPE J.* **2**, p. 56.

Walsh, M.P. and Withjack, E.M.: 1993, On some remarkable observations of laboratory dispersion based on computed tomography (CT) , Paper No. CIM 93-22 presented at the CIM 1993 Annual Technical Conference in Calgary, Alberta.

Wang, S.Y., Ayral, S. and Gryte, C.C.: 1984, Computer-assisted tomography for the observation of oil displacement in porous media, *SPE J.* **2**, p. 53.

Withjack, E.M.: 1988, Computed tomography for rock-property determination and fluid-flow visualization, *SPERE* **12**, p. 696

Zhang, X.: 1993, Effect of core length on miscible displacement, MSc thesis, University of Alberta.

13. Appendix A

Additional Effluent Curves: Experimental versus Matched

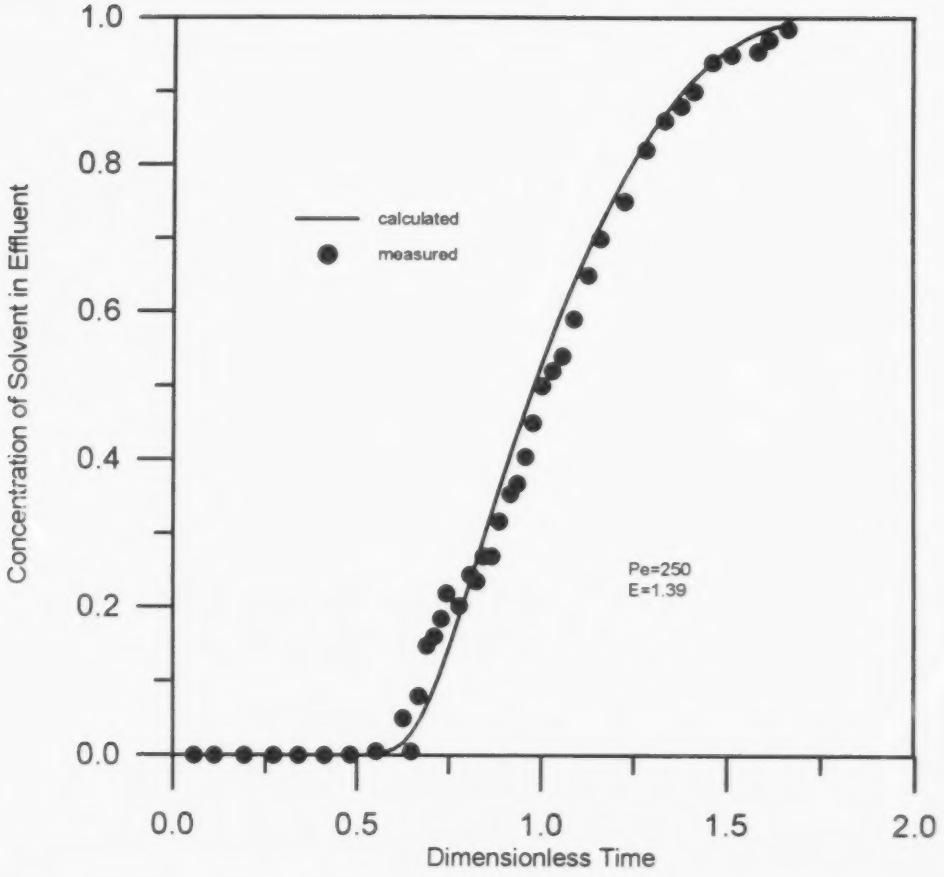

Figure A.1 Effluent Curves: Experimental versus Matched Viscosity Ratio=4.15, Velocity=0.00188 cm/s

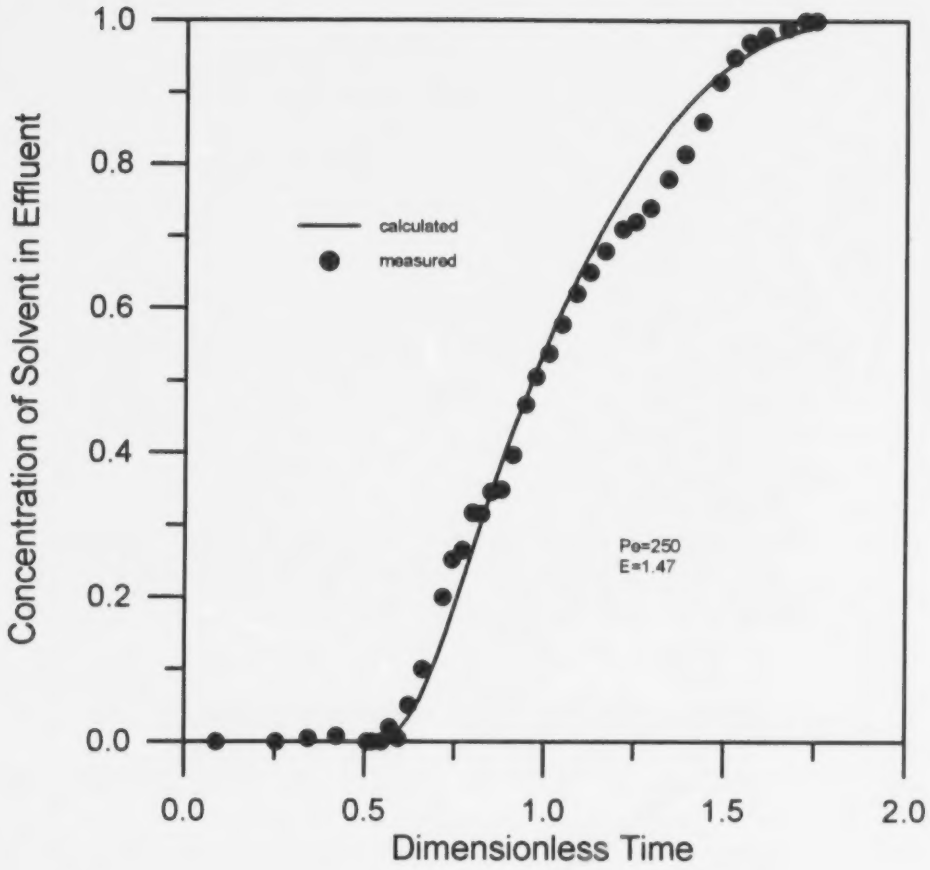

Figure A.2 Effluent Curves: Experimental versus Matched Viscosity Ratio=4.15, Velocity=0.00300 cm/s

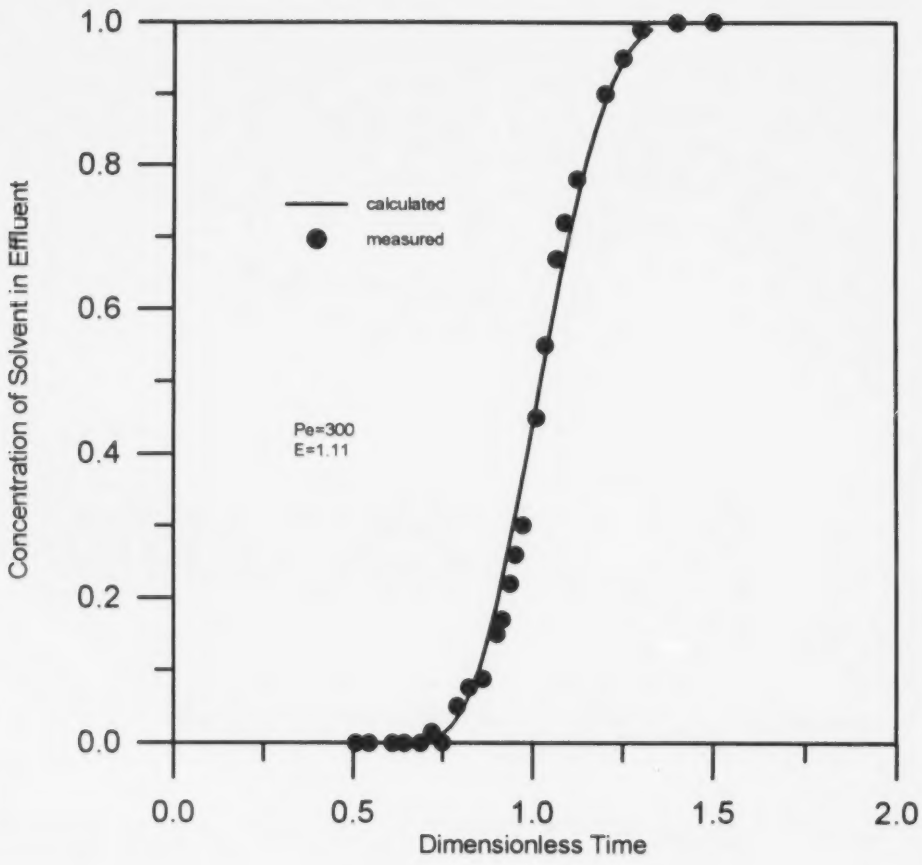

Figure A.3. Effluent Curves: Experimental versus Matched Viscosity Ratio=8.54, Velocity=0.00038 cm/s

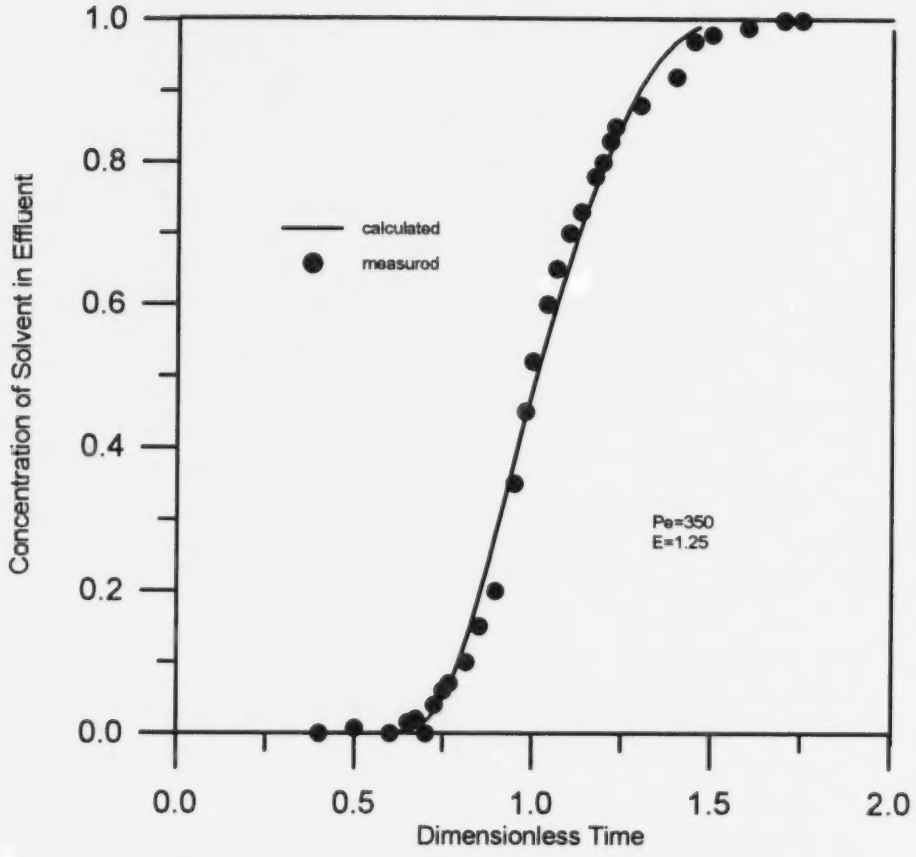

Figure A.4 Effluent Curves: Experimental versus Matched Viscosity Ratio=8.54, Velocity=0.00075 cm/s

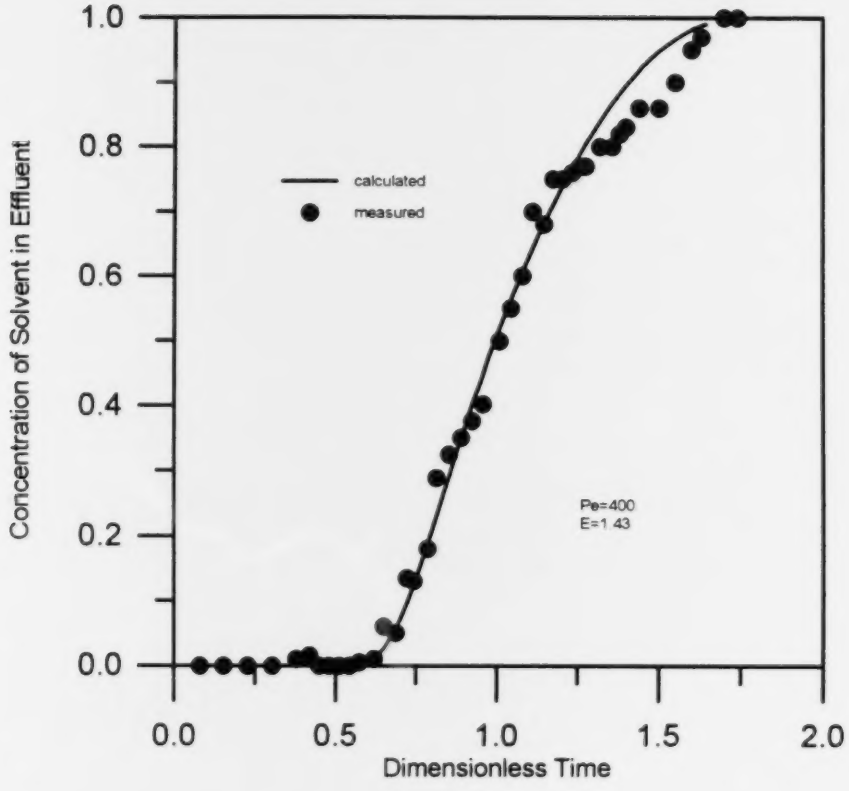

Figure A.5 Effluent Curves: Experimental versus Matched Viscosity Ratio=8.54, Velocity=0.00113 cm/s

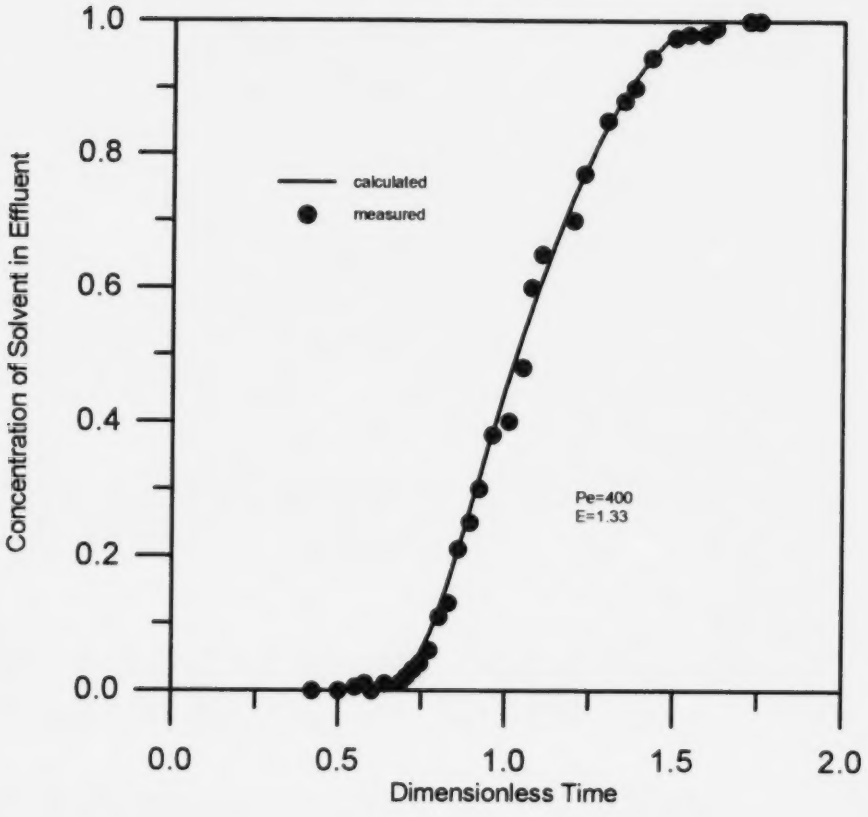

Figure A.6 Effluent Curves: Experimental versus Matched Viscosity Ratio=36.59, Velocity=0.00038 cm/s